Fracture-Matrix Interaction, Fluid Flow and Chemical Movement in Shale*

Qinhong "Max" Hu[1]

Search and Discovery Article #51564 (2019)**
Posted May 6, 2019

*Adapted from oral presentation given at 2019 AAPG Southwest Section Annual Convention, Dallas, Texas, April 6-9, 2019
 DOI:10.1306/51564Hu0219

[1]The University of Texas at Arlington, Arlington, TX (maxhu@uta.edu)

Abstract

Even after hydraulic fracturing, the issues of steep initial decline and low overall recovery of hydrocarbons (oil and gas) from fine-grained reservoirs affect the economic sustainability of shale resource development. In low-permeability unsaturated fractured shale, fluid flows predominantly through the interconnected fracture network, with some fluid imbibing into the neighboring shale matrix. Imbibition (driven by capillary pressure gradient) advectively transports chemicals from fracture into matrix. Diffusion (driven by concentration gradient) can diffusively transport chemicals into/from the matrix. Once in the matrix, sorbing chemicals can sorb onto matrix rock. All these interacting processes (imbibition, sorption, and diffusion) control fluid flow and chemical transport in fractured shale. Microscopic characteristics of porous matrix – pore shape, pore-size distribution, pore connectivity – influence macroscopic behavior of fluid flow and chemical transport and can therefore affect the fate of injected fracturing fluids, flowback and produced fluids, as well as the exploration of hydrocarbons in hydraulically-fractured shales. Using an innovative and complementary laboratory approaches, such as imbibition and diffusion tests employing nano-sized tracer recipe followed with microscale mapping of tracers, our work indicates the limited fracture–matrix interactions in fractured shale, with low pore connectivity of nm-sized shale matrix pores and the consequent limited (sub-mm near the fracture face) accessible porosity and anomalous diffusion to the stimulated fracture network and producing wellbore.

References Cited

David, C., J. Wassermann, F. Amann, D.A. Lockner, E.H. Rutter, T. Vanorio, A. Amann-Hildenbrand, J. Billiotte, T. Reuschlé, D. Lasseux, J. Fortin, R. Lenormand, A.P.S. Selvadurai, P.G. Meredith, J. Browning, T.M. Mitchell, D. Loggia, F. Nono, J. Sarout, L. Esteban, C. Davy, L. Louis, G. Boitnott, C. Madonna, E. Jahns, M. Fleury, G. Berthe, P. Delage, P. Braun, D. Grégoire, L. Perrier, P. Polito, Y. Jannot, A. Sommier, B. Krooss, R. Fink, Q. Hu, J. Klaver, and A. Clark, 2018, KG²B, A Collaborative Benchmarking Exercise for Estimating the Permeability of the Grimsel Granodiorite – Part 1: Measurements, Pressure Dependence, and Pore-Fluid Effects: Geophysical Journal International, v. 215/2, p. 799-824. doi.org/10.1093/gji/ggy304

David, C., J. Wassermann, F. Amann, J. Klaver, C. Davy, J. Sarout, L. Esteban, E.H. Rutter, Q. Hu, L. Louis, P. Delage, D.A. Lockner, A.P.S. Selvadurai, T. Vanorio, A. Amann-Hildenbrand, P.G. Meredith, J. Browning, T.M. Mitchell, C. Madonna, J. Billiotte, T. Reuschlé, D. Lasseux, J. Fortin, R. Lenormand, D. Loggia, F. Nono, G. Boitnott, E. Jahns, M. Fleury, G. Berthe, P. Braun, D. Grégoire, L. Perrier, P. Polito, Y. Jannot, A. Sommier, B. Krooss, R. Fink, and A. Clark, 2018, KG²B, A Collaborative Benchmarking Exercise for Estimating the Permeability of the Grimsel Granodiorite - Part 2: Modelling, Microstructures, and Complementary Data: Geophysical Journal International, v. 215,/2, p. 825843. doi.org/10.1093/gji/ggy305

Loucks, R.G., R.M. Reed, S.C. Ruppel, and D.M. Jarvie, 2009, Morphology, Genesis, and Distribution of Nanometer-Scale Pores in Siliceous Mudstones of the Mississippian Barnett Shale: Journal of Sedimentary Research, v. 79, p. 848-861. doi:10.2110/jsr.2009.092

Hu, Q., R.P. Ewing, and S. Dultz, 2012, Pore Connectivity in Natural Rock: Journal of Contaminant Hydrology, v. 133, p. 76-83. doi:10.1016/j.jconhyd.2012.03.006

Hu, Q., R.P. Ewing, and H.D. Rowe, 2015, Low Nanopore Connectivity Limits Gas Production in Barnett Formation: Journal of Geophysical Research – Solid Earth, v. 120/12, p. 8073-8087.

Hu, Q., T.J. Kneafsey, R.C. Trautz, and J.S.Y. Wang, 2002, Tracer Penetration into Welded Tuff Matrix from Flowing Fractures: Vadose Zone Journal, v. 1, p. 102-112.

Hu, Q., X. Liu, S. Dultz, R.P. Ewing, and H.D. Rowe, 2010, Fracture-Matrix Interaction and Gas Recovery in the Barnett Shale: AAPG Hedberg Conference, December 5-10, 2010, Austin, Texas, 4 p.

Hu, Q., H. Liu, R. Yang, Y.X. Zhang, G. Kibria, S. Sahi, N. Alatrash, F.M. MacDonnell, and W. Chen, 2017, Applying Molecular and Nanoparticle Tracers to Study Wettability and Connectivity of Longmaxi Formation in Southern China: Journal of Nanoscience and Nanotechnology, v. 17, p. 6284-6295.

Hu, Q., Y.X. Zhang, X.H. Meng, Z. Li, Z.H. Xie, and M.W. Li, 2017, Characterization of Multiple Micro-Nano Pore Networks in Shale Oil Reservoirs of Paleogene Shahejie Formation in Dongying Sag of Bohai Bay Basin, East China: Petroleum Exploration and Development, v. 44/5, p. 720-730.

Hu, Q.H., W. Zhou, P. Huggins, and W.L. Chen, 2018, Pore Structure and Fluid Uptake of the Goddard Shale Formation in Southeastern Oklahoma, USA: Geofluids, Article ID 5381735.

Nelson, P.H., 2009, Pore-Throat Sizes in Sandstones, Tight Sandstones, and Shales: American association of Petroleum Geologists Bulletin, v. 93, p. 329-340.

Sun, M., B. Yu, Q. Hu, R. Yang, Y. Zhang, B. Li, Y.B. Melnichenko, and G. Cheng, 2017, Pore Structure Characterization of Organic-Rich Niutitang Shale from China: Small Angle Neutron Scattering (SANS) Study: International Journal of Coal Geology, v. 186, p. 115-125. dio:10.1016/j.coal.2017.12.006

Sun, M., B. Yu, Q. Hu, Y. Zhang, B. Li, R. Yang, Y.B. Melnichenko, and G. Cheng, 2017, Pore Characteristics of Longmaxi Shale Gas Reservoir in the Northwest of Guizhou, China: Investigations Using Small-Angle Neutron Scattering (SANS), Helium Pycnometry, and Gas Sorption Isotherm: International Journal of Coal Geology, v. 171, p. 61-68.

Walls, J., A. Morcote, T. Hintzman, and M. Everts, 2016, Comparative Core Analysis from a Wolfcamp Formation Well; A Case Study: International Symposium of the Society of Core Analysts held in Snow Mass, Colorado, USA, 21-26 August 2016, SCA2016-044, 6 p.

Yang, R., S. He, Q. Hu, M. Sun, D. Hu, and J. Yi, 2017, Applying SANS Technique to Characterize Nano-Scale Pore Structure of Longmaxi Shale, Sichuan Basin (China): Fuel, v. 197, p. 91-99.

Zhang et al., 2019, Small Angle Neutron Scattering, in press.

Zhao, J.H., Z.J. Jin, Q.H. Hu, Z.K. Jin, T.J. Barber, Y.X. Zhang, and M.K. Bleuel, 2017, Integrating SANS and Fluid-Invasion Methods to Characterize Pore Structure of Typical American Shale Oil Reservoirs: Scientific Reports, v. 7, p. 15413.

UNIVERSITY OF TEXAS ARLINGTON

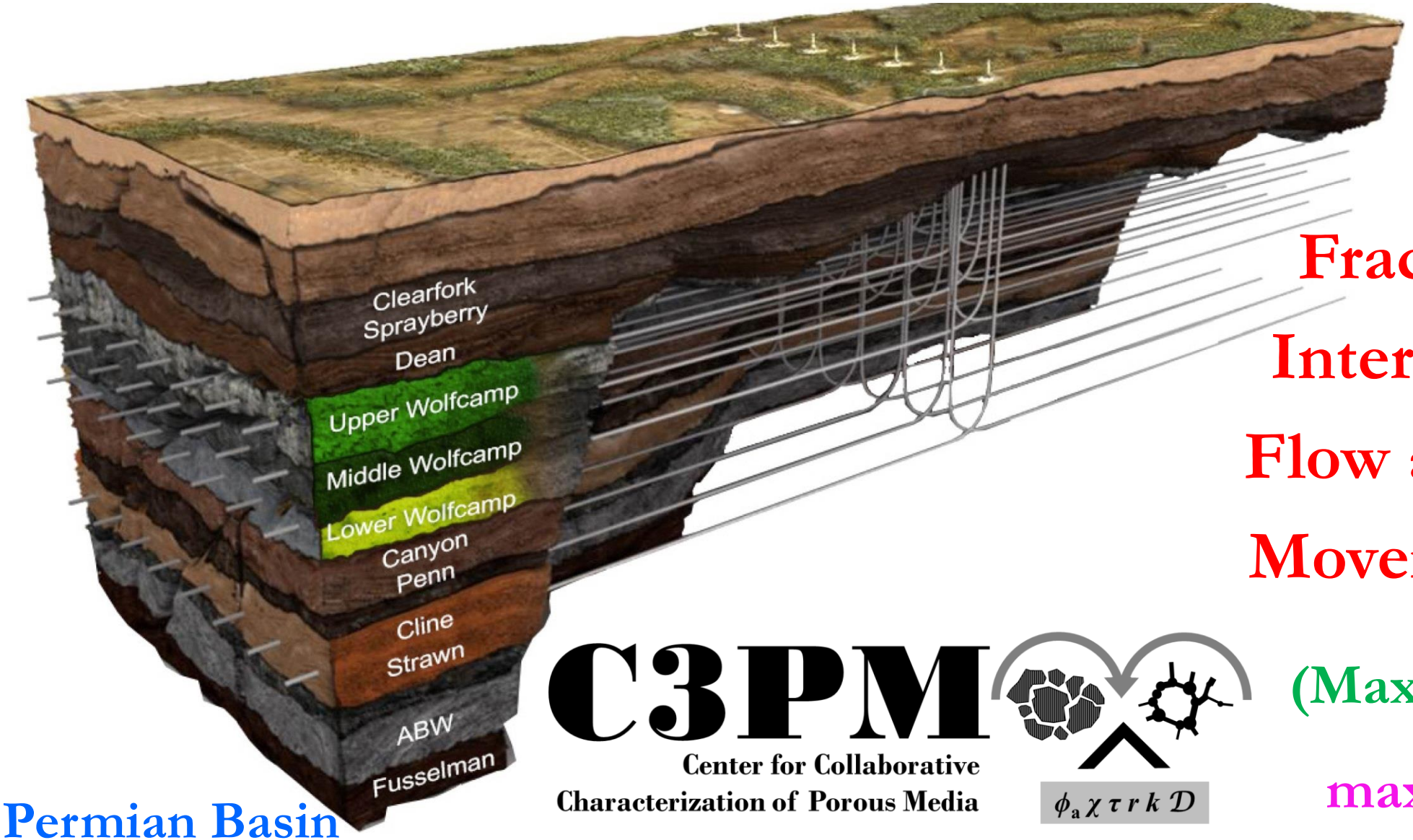

Permian Basin

Fracture-matrix Interaction, Fluid Flow and Chemical Movement in Shale

C3PM
Center for Collaborative Characterization of Porous Media

$\phi_a \chi \tau r k \mathcal{D}$

(Max) Qinhong Hu

maxhu@uta.edu

UNIVERSITY OF TEXAS ARLINGTON

Outline

- Production decline and fracture-matrix interaction
- Scientific issues across scales
  - ✓ Connectivity
  - ✓ Wettability
  - ✓ Accessibility
  - ✓ Diffusivity
  - ✓ Tortuosity
  - ✓ Permeability
  - ✓ Capillarity
  - ✓ Fracability
  - ✓ Productivity
- Summary

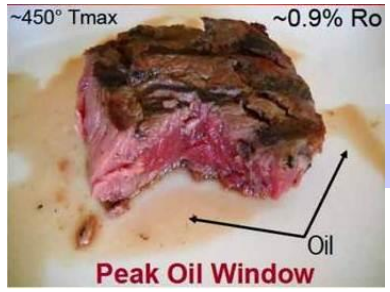

Maturity

Mixed wettability

Fracability

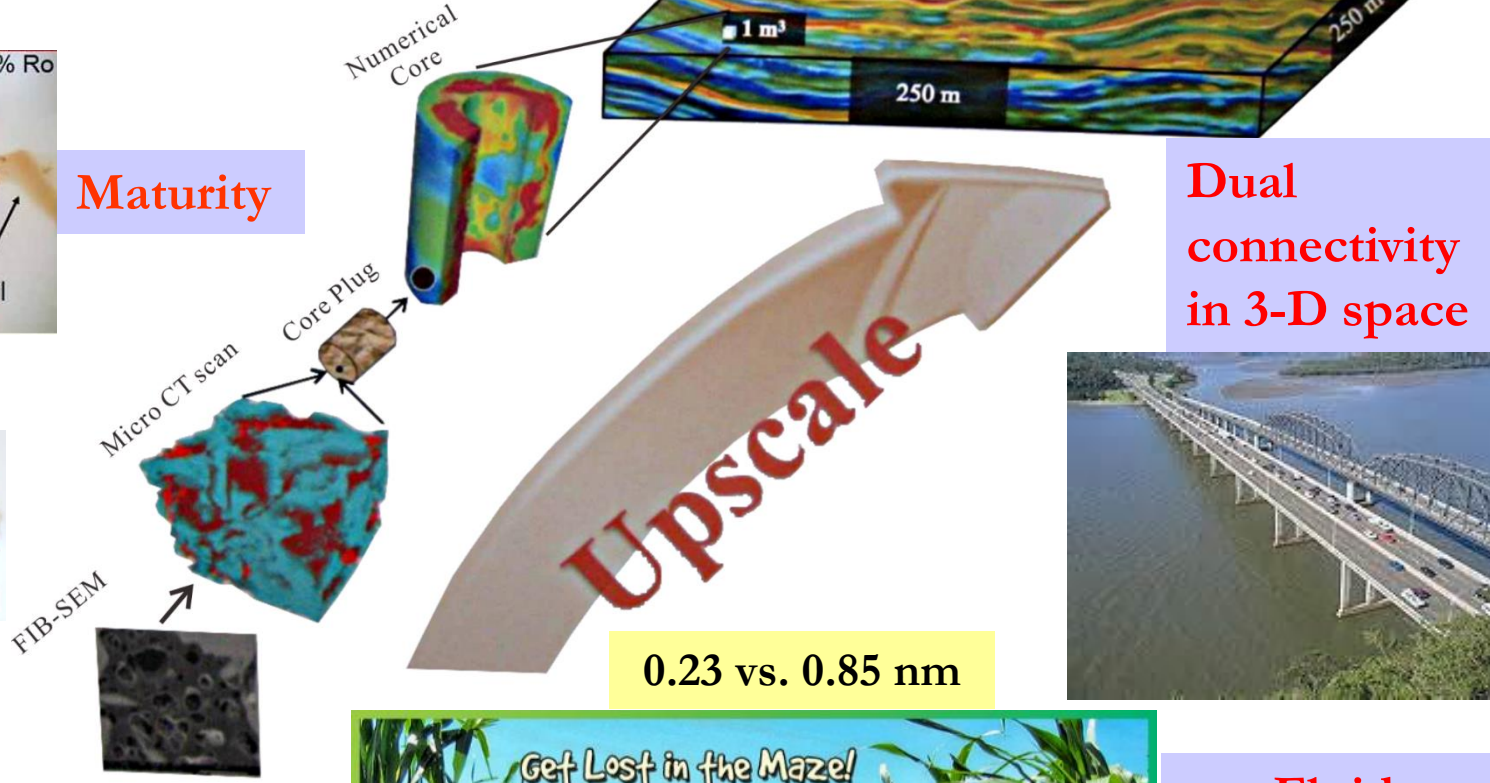

0.23 vs. 0.85 nm

Dual connectivity in 3-D space

Fluid movement in 2-D space

UNIVERSITY OF TEXAS ARLINGTON

Ongoing Shale Revolution

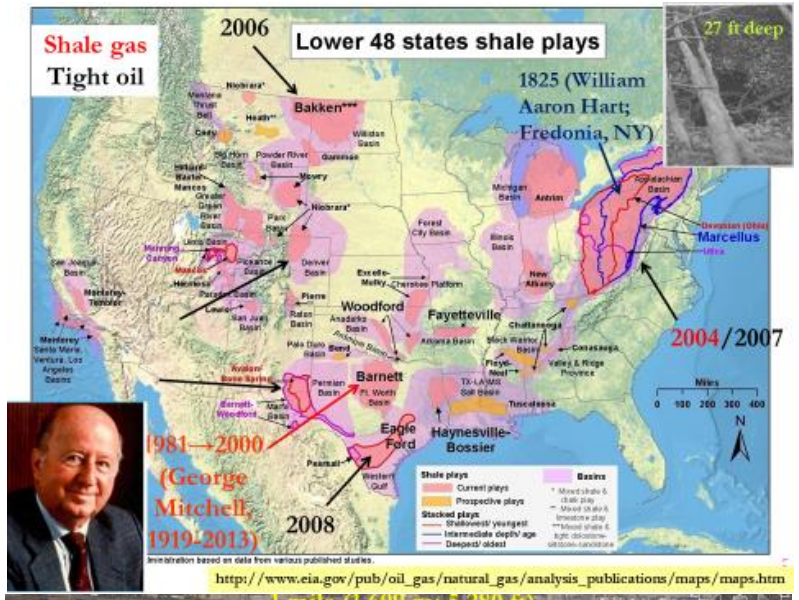

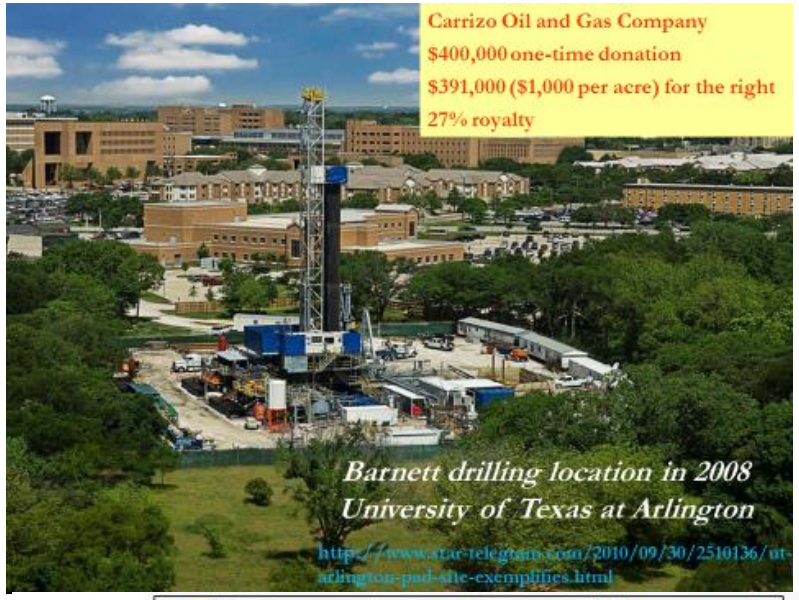

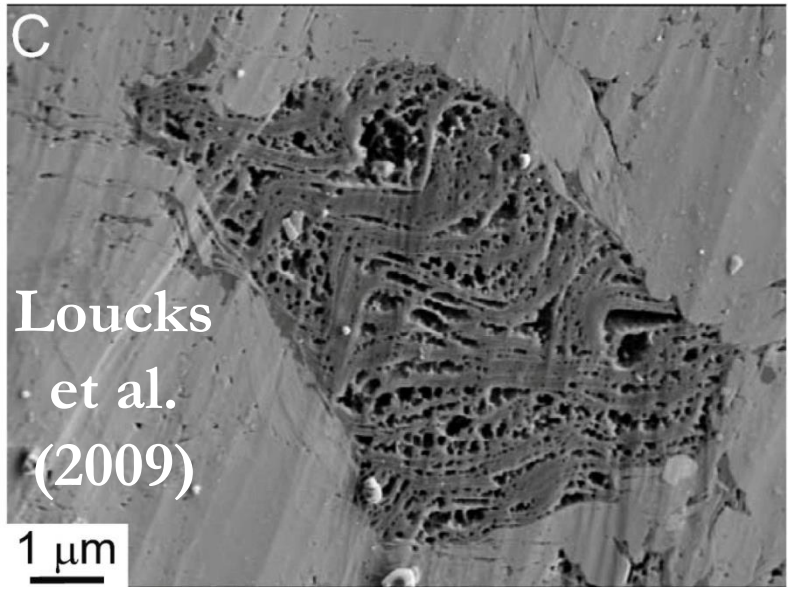

http://www.eia.gov/todayinenergy/detail.cfm?id=2170

Updated June 1, 2011

A total of 17,685 wells (early 2013) by 250+ companies

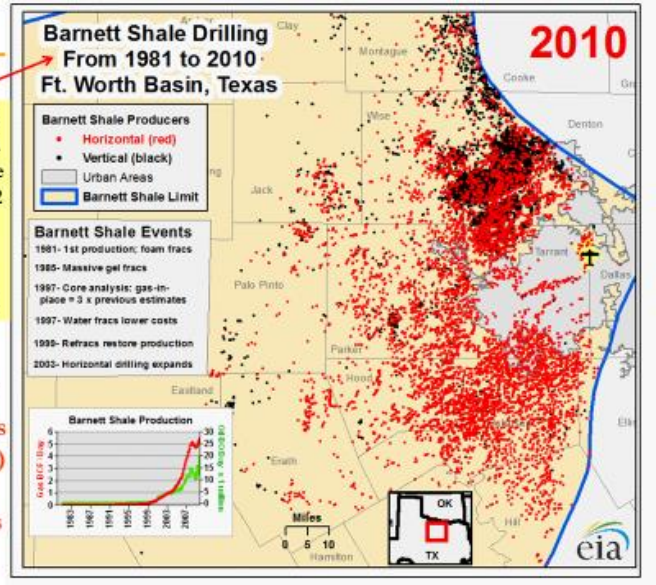

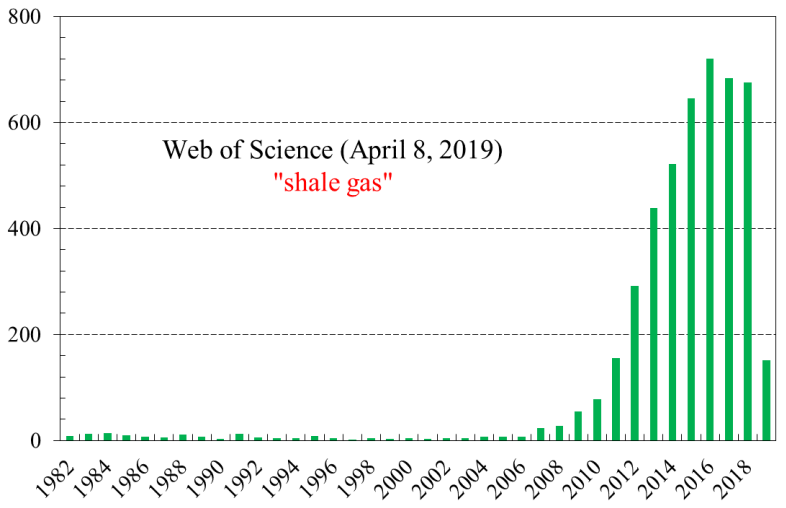

UNIVERSITY OF TEXAS ARLINGTON

Shale Revolution: Facts

Production history of 1st shale gas well

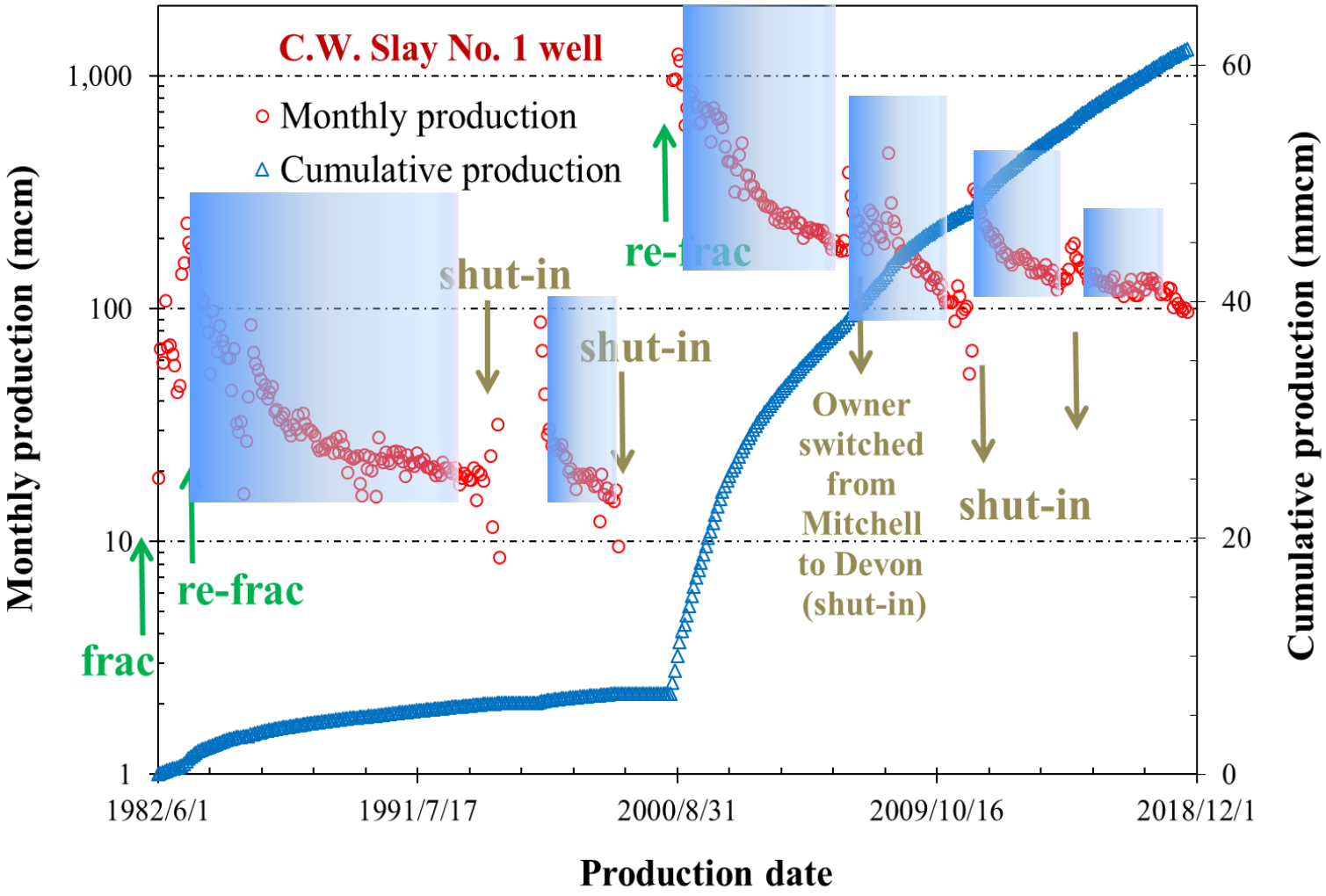

- Steep initial decline (both gas and oil: ↓ 2/3 after 1 yr)
- Low recovery (shale gas: <30%; tight oil: <10%)
- 40% wells (~90,000) drilled in US uneconomic
- 25% wells produce ~80% output ("80-20 Rule")

UNIVERSITY OF TEXAS ARLINGTON

Hypothesis: Fracture-matrix Interactions Control Production Behavior in Stimulated Shale

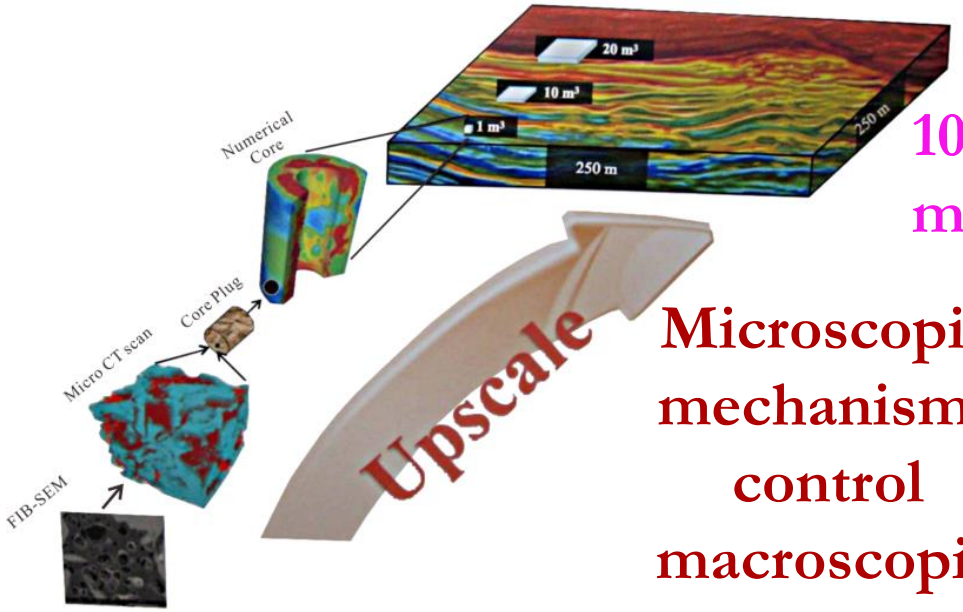

10+ orders of magnitude in scale

Microscopic mechanisms control macroscopic production

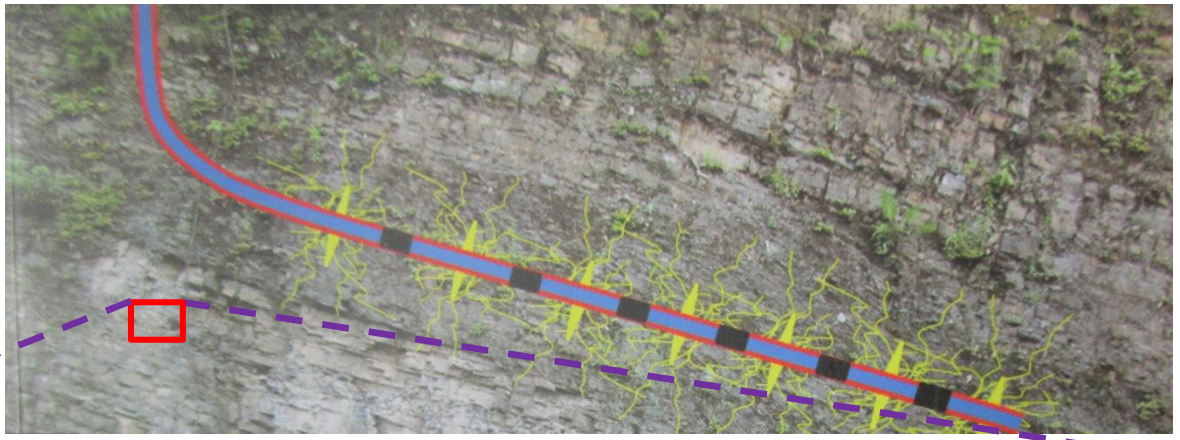

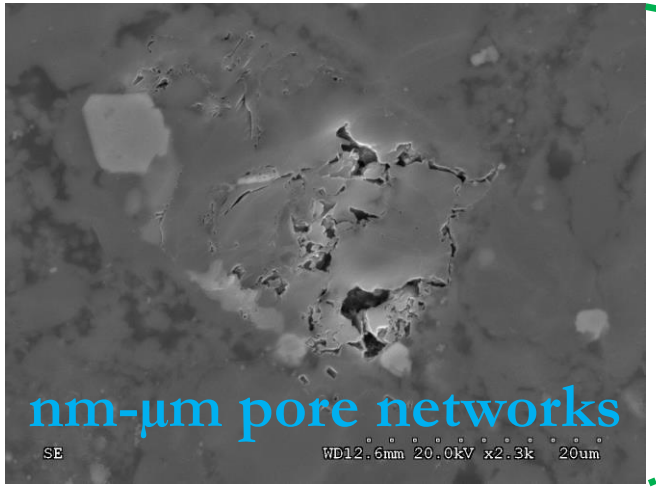

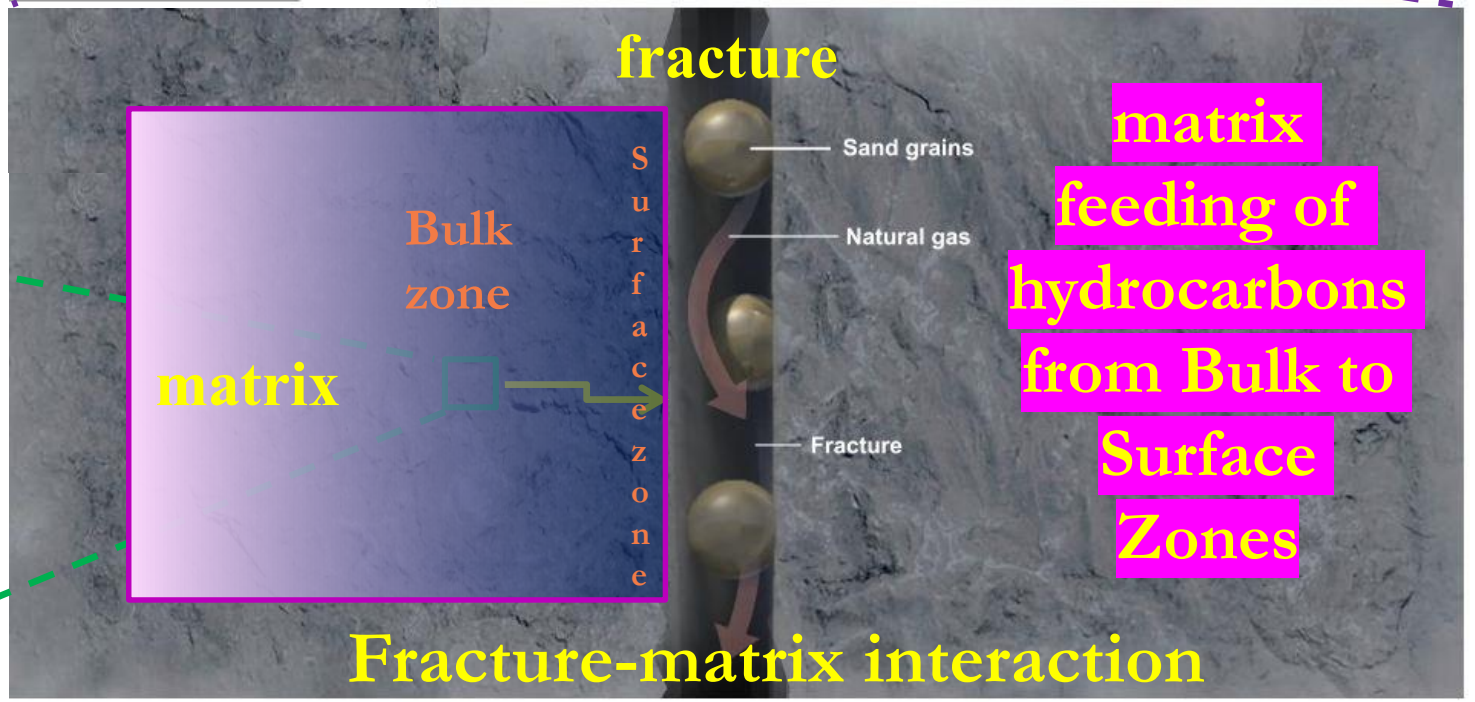

UNIVERSITY OF TEXAS ARLINGTON

Earlier Fracture-Matrix (F-M) Interaction Studies

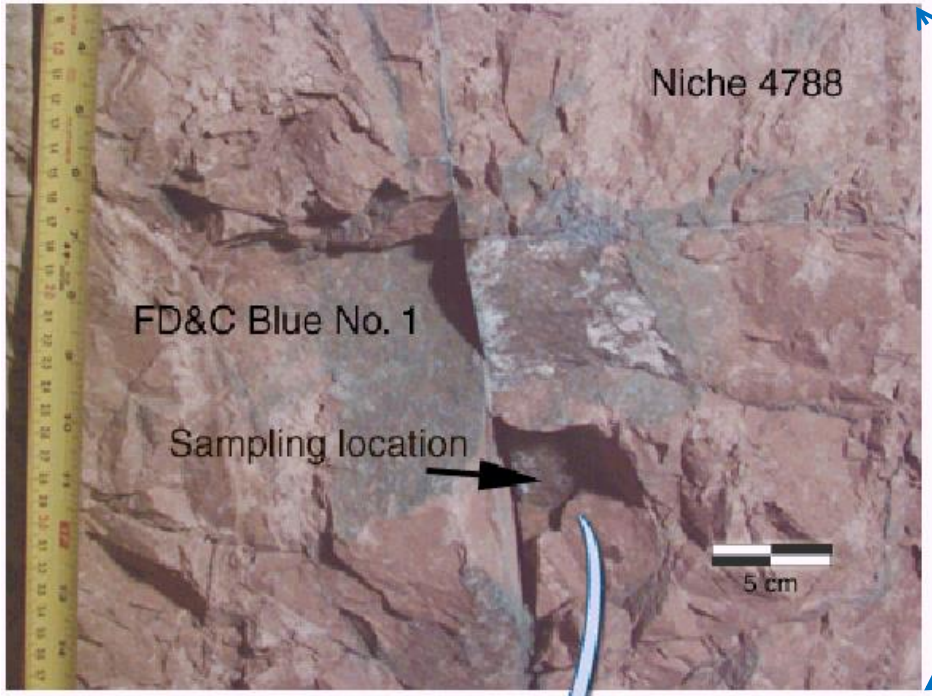

Field observation (preferential flow in a fracture network) of dye distribution in unsaturated fractured tuff at Yucca Mt.

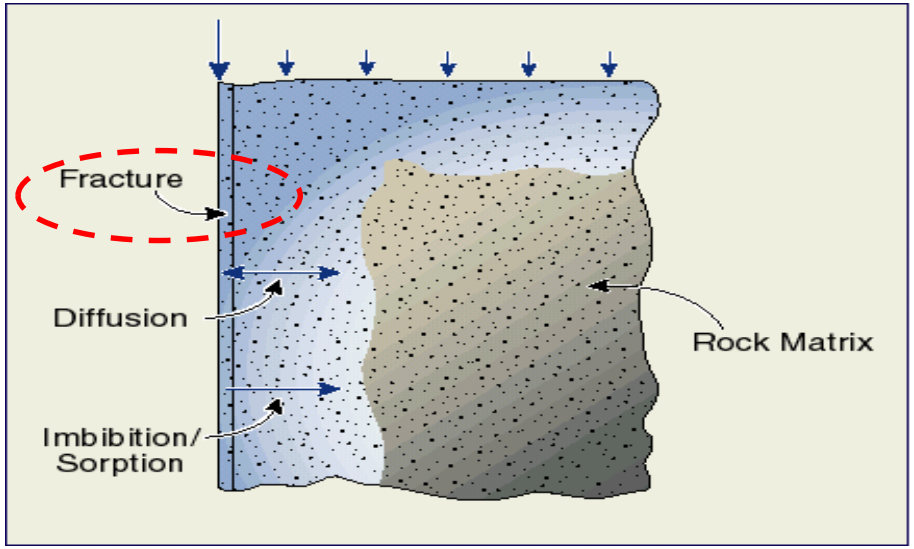

Rock milling in 1998

My work on fracture-matrix interaction starts with this rock

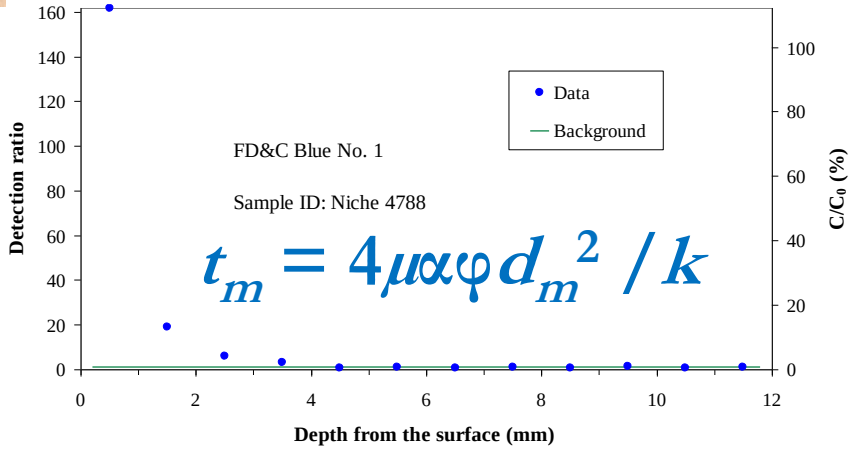

UNIVERSITY OF TEXAS ARLINGTON

Pore Structure: Geometry and Topology

Percolation theory: the mathematics of how macroscopic properties emerge from local (microscopic) connections

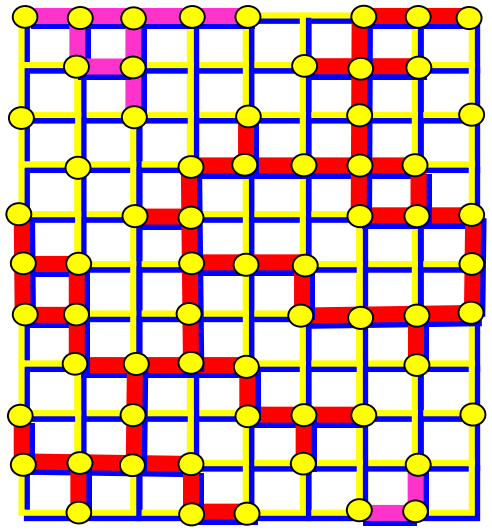

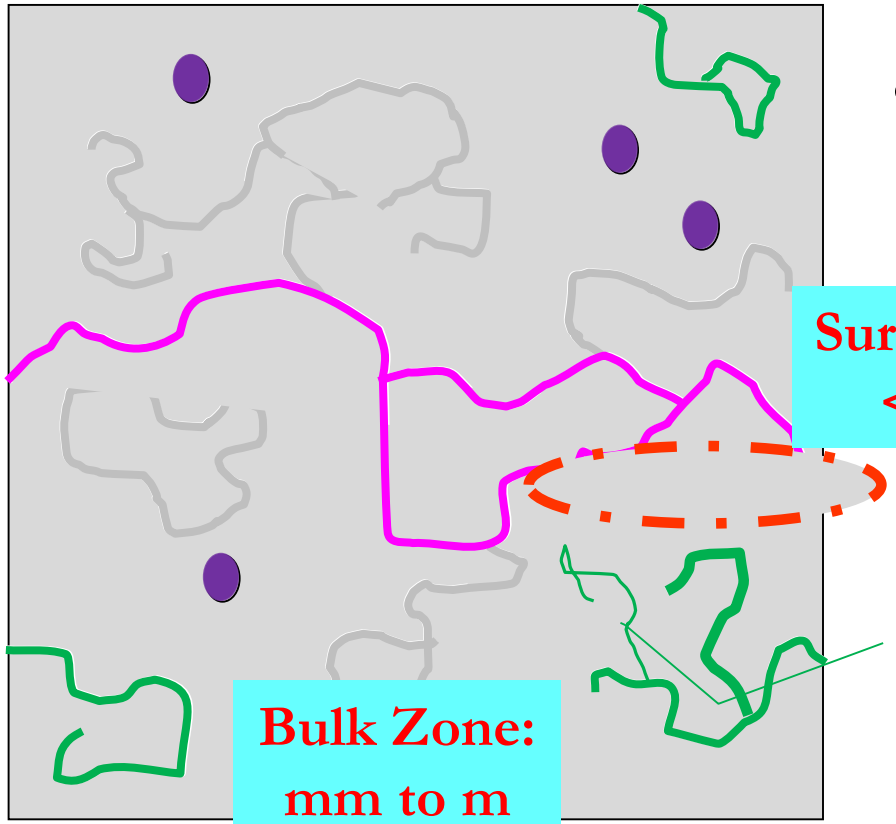

- Total Porosity
  - Isolated Porosity
  - Connected Porosity
    - Edge Porosity
    - Infinite Cluster
      - Backbone
      - Dead Ends

Effective porosity/Total porosity (ϕ_e/ϕ)

Surface Zone: ~70% Bulk Zone: ~0.1%)

Unique Dual-Connectivity Zones of Shale: Multiple Evidence

Wood's metal impregna-tion (600 MPa)

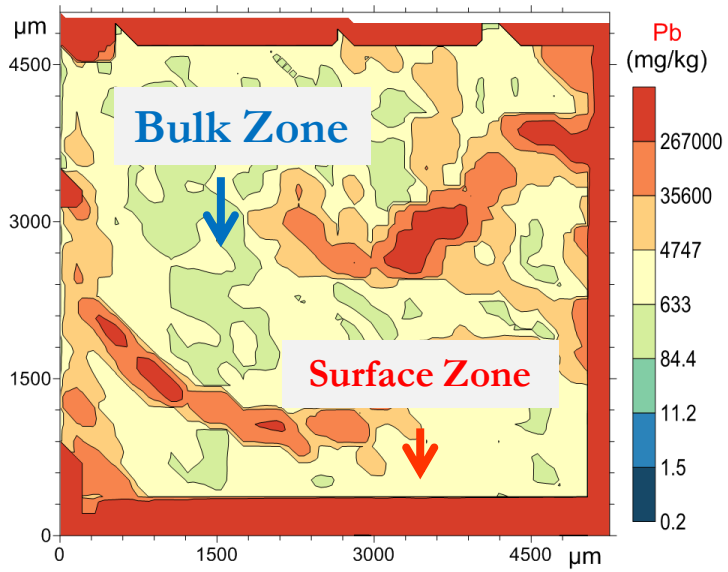

Diffusion

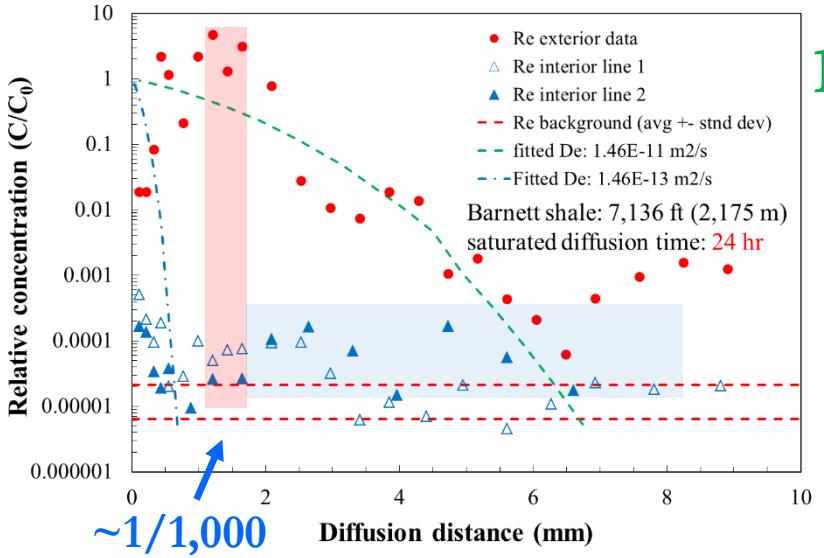

Imbibition

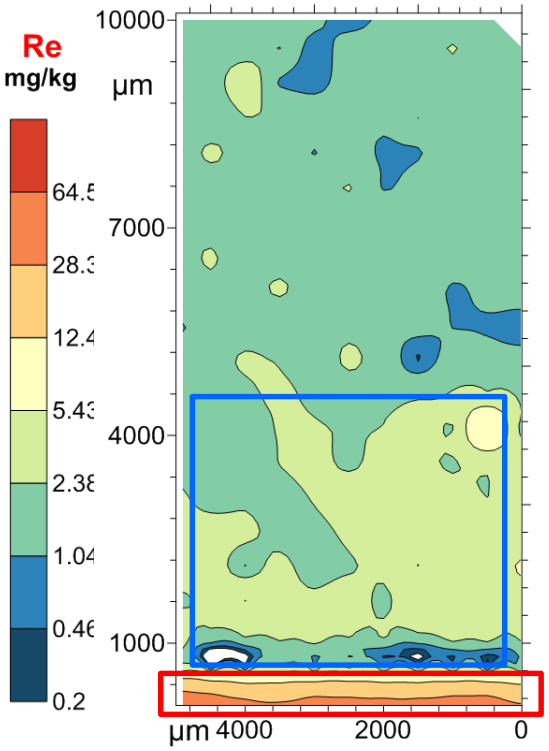

1 cm cube

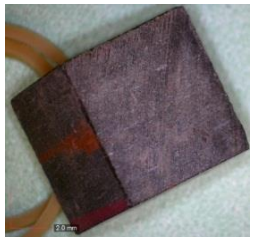

Size GRI (500-841 μm)

MICP

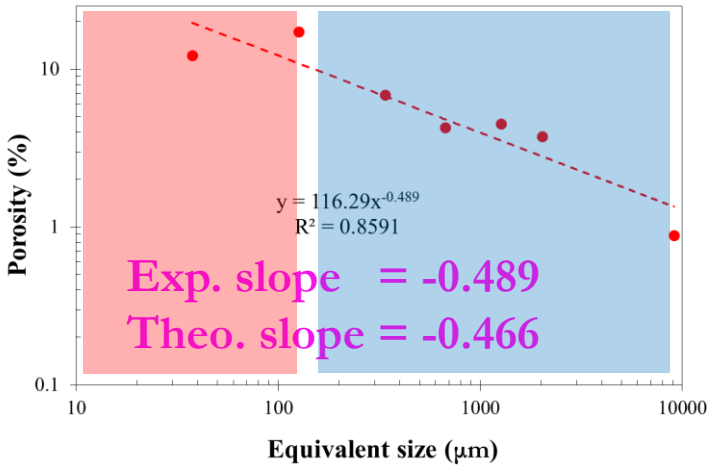

Size B (177-500 μm)

Size C (75-177 μm)

UNIVERSITY OF TEXAS ARLINGTON

Edge-accessible Effective Porosity

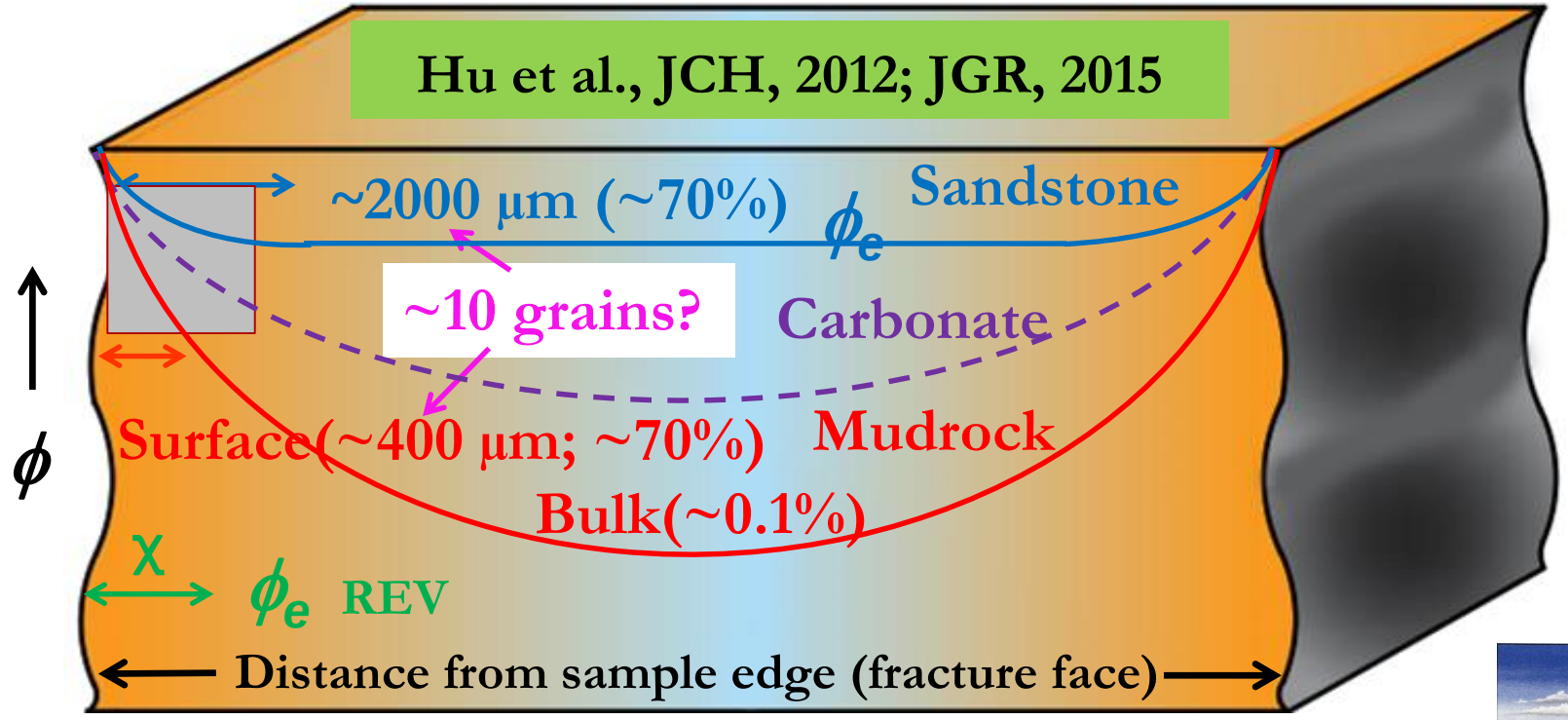

- Larger proportion of closed pores for larger sample sizes
- Assess pore connectivity by measuring effective porosity of different sample sizes

up-scaling (percolation)

$$\phi(h) = \phi_e \begin{cases} (h/\chi)^{\beta/\nu} & h < \chi \\ 1 & h > \chi \end{cases}$$

χ : correlation length

β and υ: percolation exponents — 0.41 and 0.88 for 3-D

UNIVERSITY OF TEXAS ARLINGTON

Multiple Approaches to Studying Pore Structure (Geometry and Topology)

- Pycnometry of gas and hydrophilic / hydrophobic fluids (DI water; API brine; n-decane; isopropyl alcohol IPA or tetrahydrofuran THF) for fluid-accessible effective porosity of a range of sample sizes (μm – 10 cm) (UTA)
- Fluid (DI water; API brine; n-decane; IPA or THF) and tracer imbibition with respect to sample bedding direction and initial moisture content (UTA)
- Edge-accessible porosity after tracer vacuum-saturation and high-pressure intrusion (UTA)
- Liquid and gas diffusion, under ambient *and high-pressure / high-temperature* conditions (UTA)
- Mercury Injection Capillary Pressure analysis and hysteresis (UTA; CUG)
- Low-pressure gas adsorption isotherm and hysteresis (Univ. of Tokyo, Japan; CDUT, CAS-GIG and CUG, China; UT Austin; Kansas State Univ.)
- Water vapor adsorption isotherm and hysteresis (UTA)
- Nuclear Magnetic Resonance Cryoporometry (Lab-Tools, Ltd., UK; Niumag Co., China; UPC)
- Ar ion milling Field Emission-SEM (FE-SEM) and QEMSCAN (Quantitative Evaluation of Materials by Scanning) mapping, correlated with tracer mapping to study Dalmatian wettability and connectivity of shale composition pore systems (Hitachi; CUP-Beijing, CAS-GIG, and CGS-O&G, China)
- 2-D imaging/mapping after Wood's metal impregnation (Univ. Hannover, Germany; EPMA, Switzerland)
- Microtomography (high-resolution, synchrotron, nano-CT) (PNNL-EMSL; Swiss Light Source; Univ. Hannover; Saitama Univ., Japan; CUP-Beijing, RIPED, China)
- Focused Ion Beam/SEM (FIB-SEM) imaging (PNNL-EMSL; CUP-Beijing; CGS-O&G)
- Small-Angle Neutron Scattering (U)SANS (NIST; ORNL; LANL; Mianyang) and Small-Angle X-Ray Scattering (Shanghai SSRF; Beijing BSRF, Jilin Univ., China)
- Pore-scale network modeling (Iowa State Univ.; Wright State Univ.; Kansas State Univ.)
- Physics-based production decline analyses (DrillingInfo; IHS-Fekete Harmony; *Eclipse*; *Kappa*)

Hu et al., Hedberg, 2010

UNIVERSITY OF TEXAS ARLINGTON

Pore Structure, Wettability, and Hydrocarbon Movement

Accessory data

- *TOC*
- *Maturity*
- *Mineralogy*
- *Pyrolysis*
- *Well logging*
- *Production*

✓ *Gas and liquid pycnometry (different sample sizes)*

✓ *MICP (different sizes)*

✓ *Gas sorption isotherm*

✓ *(U)SANS*

✓ *NMRc*

✓ *GRI matrix k*

✓ *FE-SEM*

✓ *FIB-SEM*

✓ *Wood's metal*

✓ *Vacuum saturation for edge-accessible porosity*

✓ *Imbibition*

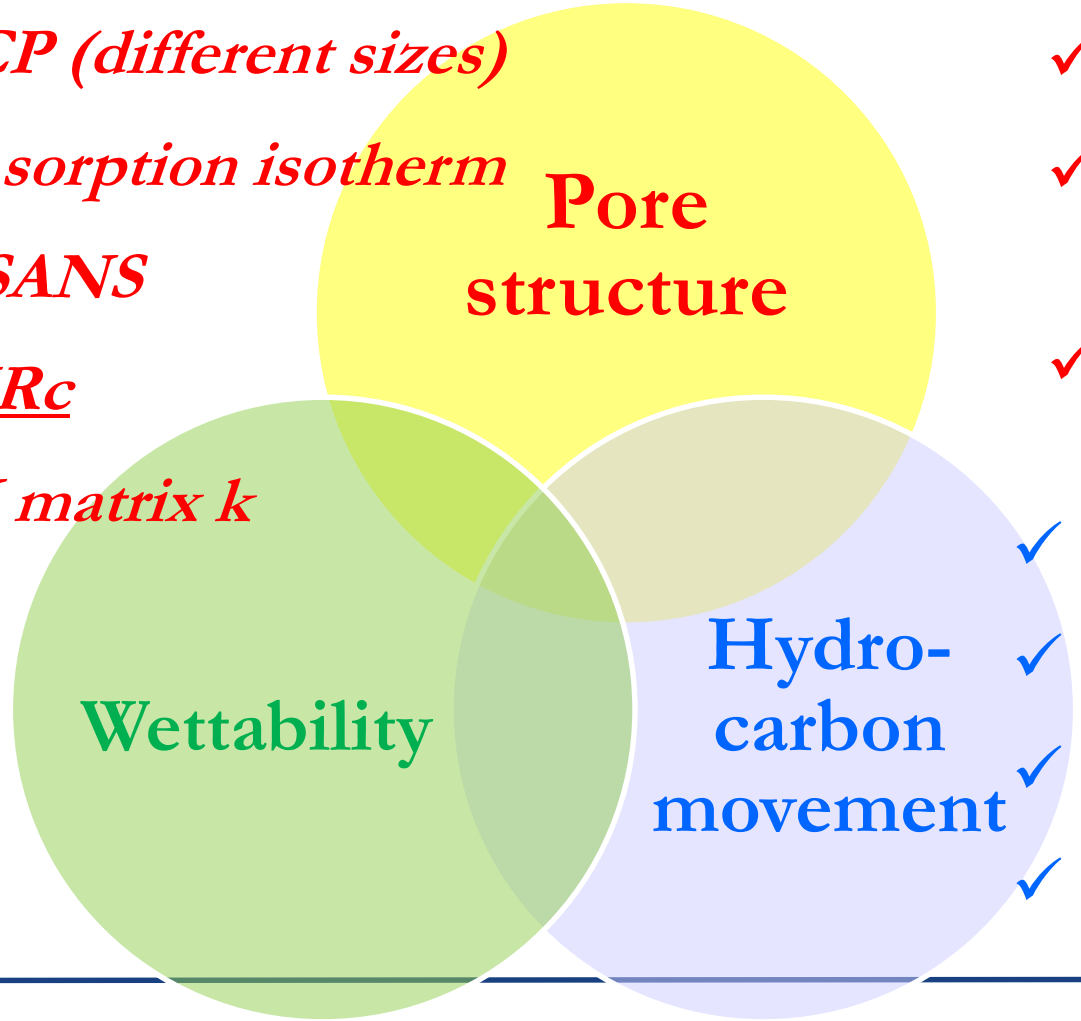

✓ *Contact angle*

✓ *Imbibition*

✓ *QEMSCAN for Dalmatian pattern*

✓ *Wettability tracers*

✓ *Imbibition*

✓ *Diffusion*

✓ *Core & m-block flooding*

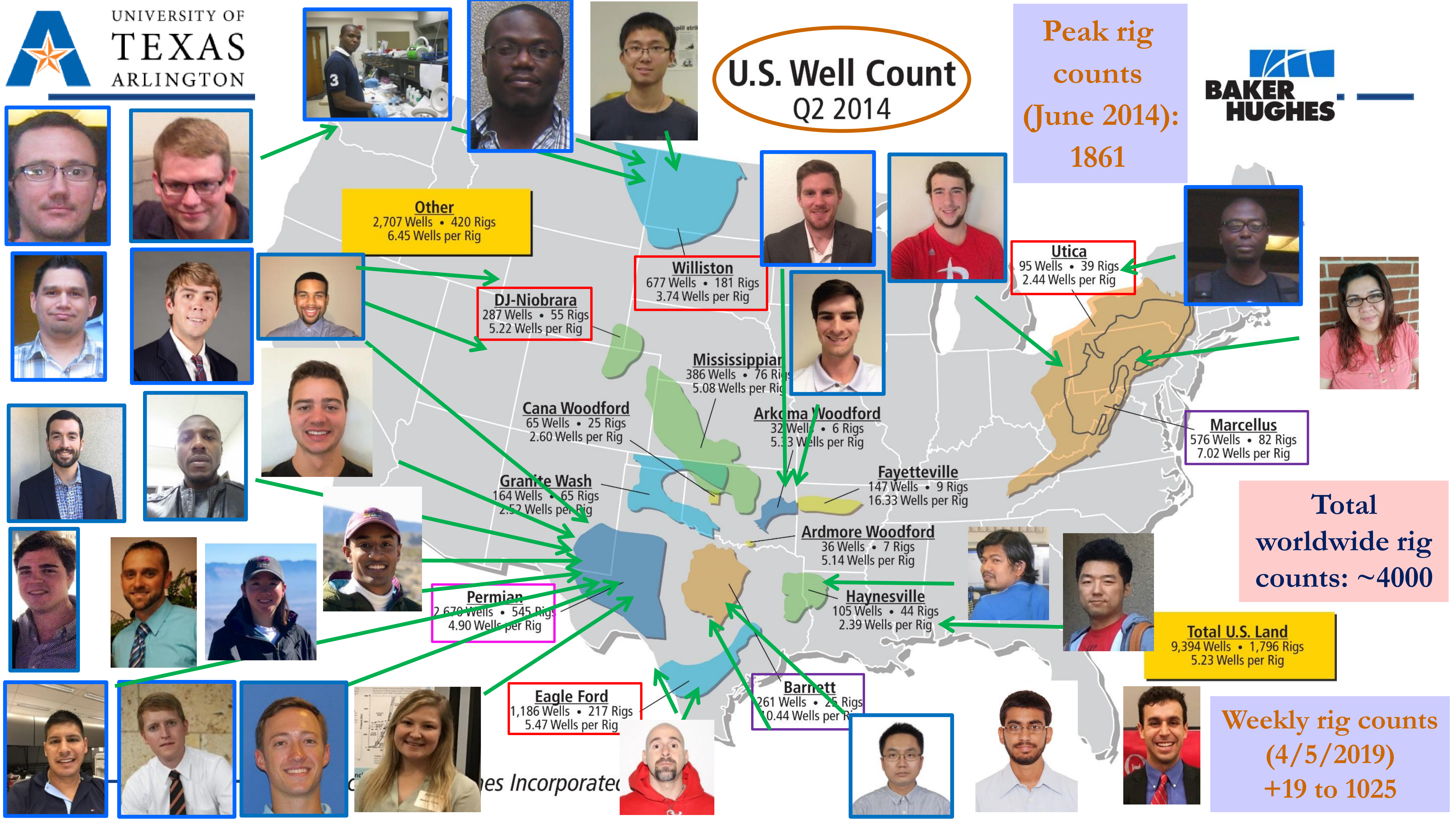

UNIVERSITY OF TEXAS ARLINGTON
U.S. Well Count
Q2 2014
Peak rig counts (June 2014): 1861
BAKER HUGHES
Other
2,707 Wells • 420 Rigs
6.45 Wells per Rig
Williston
677 Wells • 181 Rigs
3.74 Wells per Rig
DJ-Niobrara
287 Wells • 55 Rigs
5.22 Wells per Rig
Utica
95 Wells • 39 Rigs
2.44 Wells per Rig
Mississippian
386 Wells • 76 Rigs
5.08 Wells per Rig
Cana Woodford
65 Wells • 25 Rigs
2.60 Wells per Rig
Arkoma Woodford
32 Wells • 6 Rigs
5.33 Wells per Rig
Marcellus
576 Wells • 82 Rigs
7.02 Wells per Rig
Fayetteville
147 Wells • 9 Rigs
16.33 Wells per Rig
Granite Wash
164 Wells • 65 Rigs
2.52 Wells per Rig
Ardmore Woodford
36 Wells • 7 Rigs
5.14 Wells per Rig
Total worldwide rig counts: ~4000
Permian
2,670 Wells • 545 Rigs
4.90 Wells per Rig
Haynesville
105 Wells • 44 Rigs
2.39 Wells per Rig
Total U.S. Land
9,394 Wells • 1,796 Rigs
5.23 Wells per Rig
Eagle Ford
1,186 Wells • 217 Rigs
5.47 Wells per Rig
Barnett
261 Wells • 25 Rigs
10.44 Wells per Rig
Weekly rig counts (4/5/2019) +19 to 1025
es Incorporated

UNIVERSITY OF TEXAS ARLINGTON

Sweet Spots and Sampling

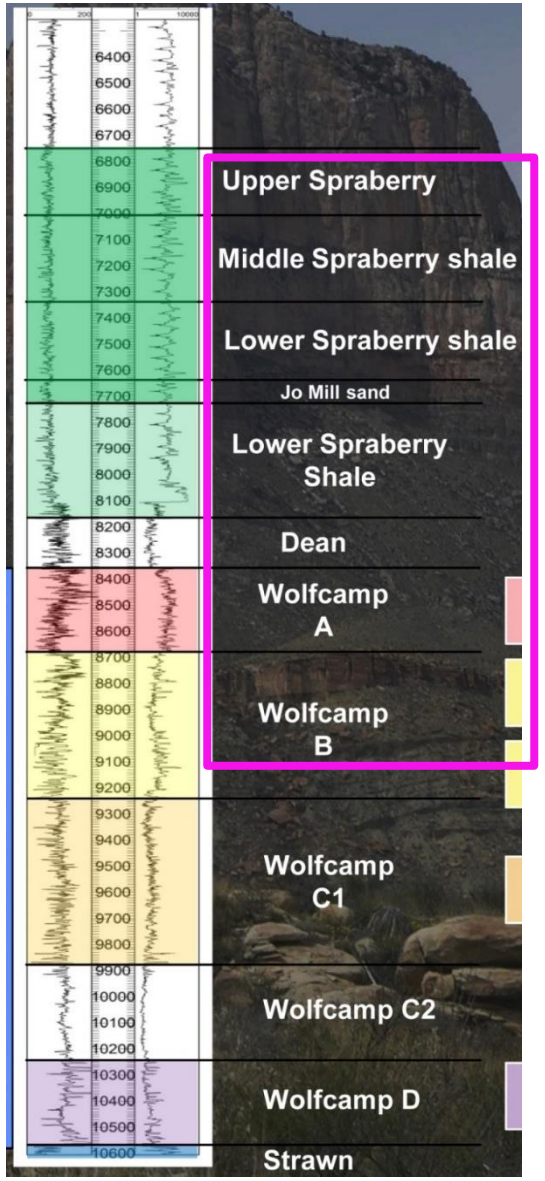

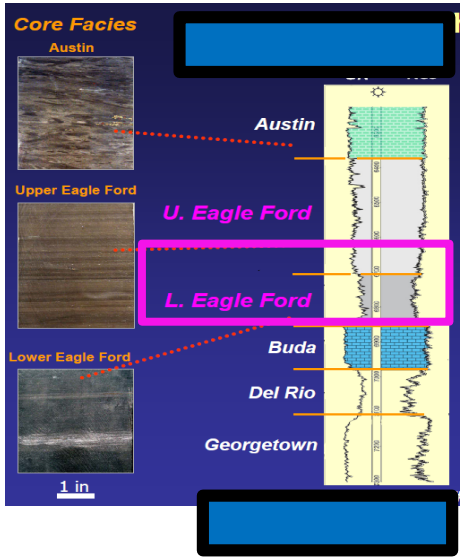

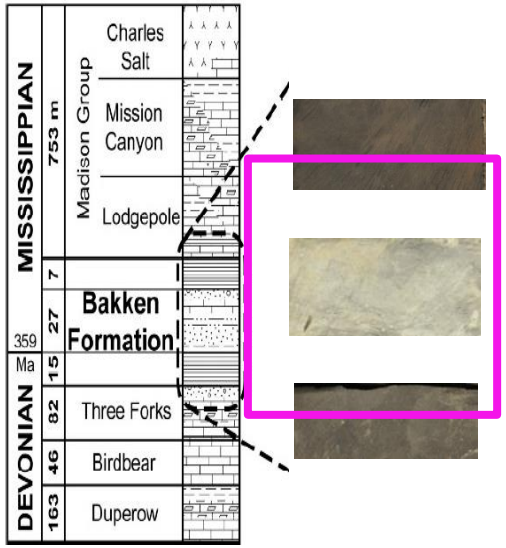

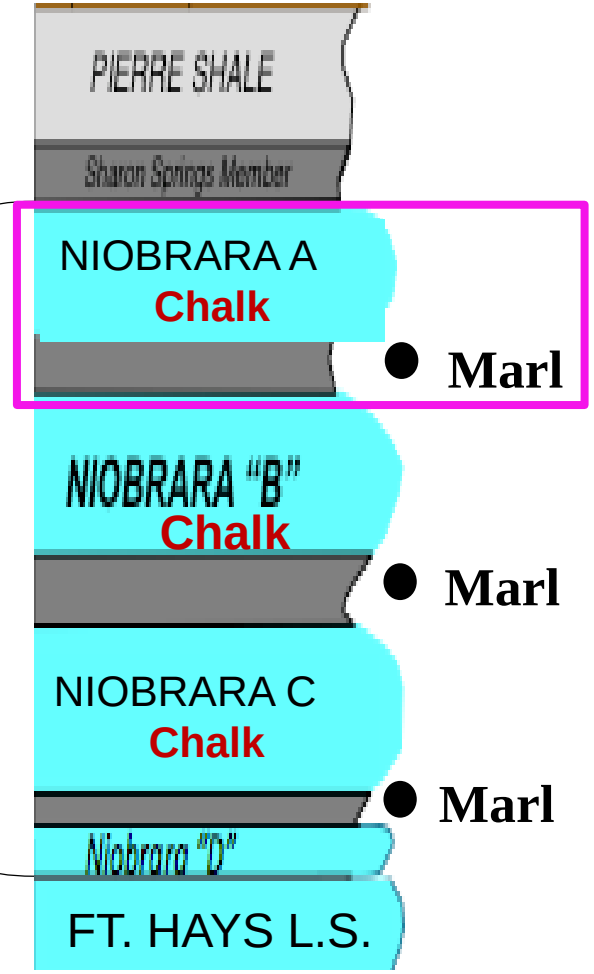

Mississippian	Chesterian	Springer Sands
		Springer Shale Goddard
	Meramec	Caney Shale
	Osagean	Sycamore Limestone
Devonian	Middle – Upper	Woodford Shale
	Ulsterian	Hunton Limestone
Silurian	Cayugan	
	Niagaran	

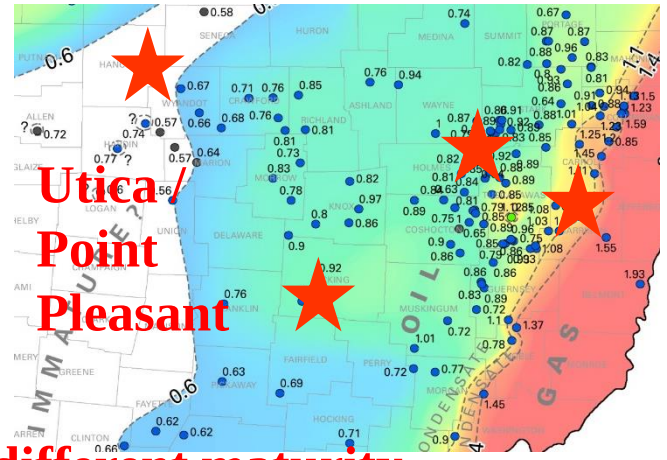

UNIVERSITY OF TEXAS ARLINGTON

Vacuum Saturation: Sample Size and Fluids

Effective porosity ↓ sample size

- Measure porosity & densities for large and irregular samples
- Use different (polar and non-polar) fluids: DI water, n-decane, toluene, isopropyl alcohol IPA or THF

UNIVERSITY OF TEXAS ARLINGTON

A Range of Sample Sizes for Different Tests

Then crush ALL fragments into different size fractions

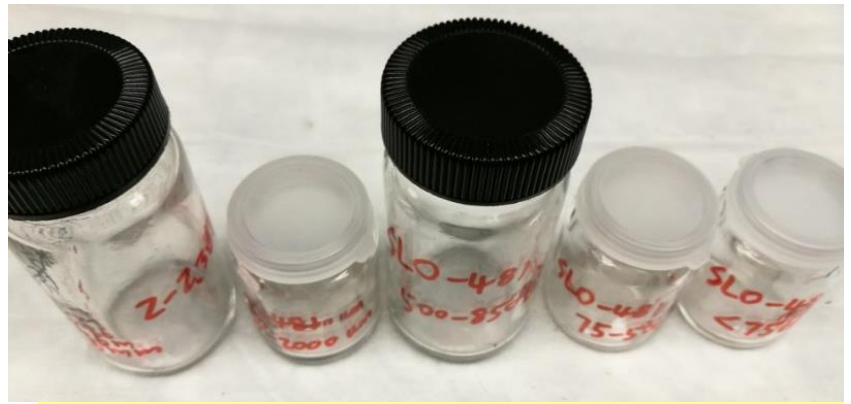

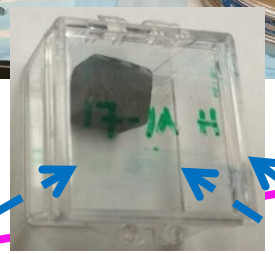

First cut as many as 15 1-cm sized cubes

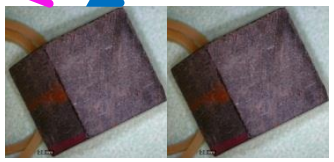

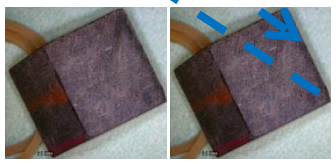

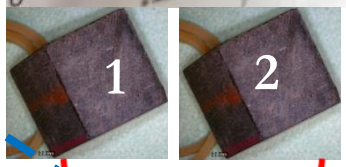

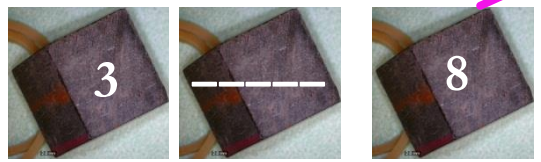

FE-SEM; SANS

220-grit sandpaper for contact angle & Ro

Epoxyed for imbibition, diffusion

Vac sat (DI water)

MICP

Vac sat (THF)

Vac sat (n-decane: toluene)

Back-up (vac sat with tracers; traced imbibition & diffusion)

UNIVERSITY OF TEXAS ARLINGTON

A Range of Sample Sizes

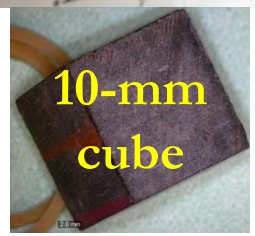

Overlaps Surface Zone and Bulk Zone for mudrocks

Size designation	Sieve mesh	Size fraction (diameter)	Equivalent spherical dia. (μm)
Cylinder / Plug		2.54 cm dia.; any height *(e.g., 3 cm)*	*(24394)*
Cube		1.0 cm	9086
Size X	8 mm to #8	2.38 - 8 mm	5190
GRI+	#8 to #12	1.70 - 2.38 mm	2040
Size A	#12 to #20	841 - 1700 μm	1271
GRI	#20 to #35	500 - 841 μm	671
Size B	#35 to #80	177 - 500 μm	339
Size C	#80 to #200	75 - 177 μm	126
Powder	<#200	< 75 μm	< 75
Size D	#200 to #625	20 - 75 μm	47.5
Size E	<635	<20 μm	<20

Global Benchmarking Tests: KG²B Project (2015-2017)

Gases vs. liquids
Steady-state vs. transient
Confining pressure

30 labs from 8 countries

1 hr – 5 d

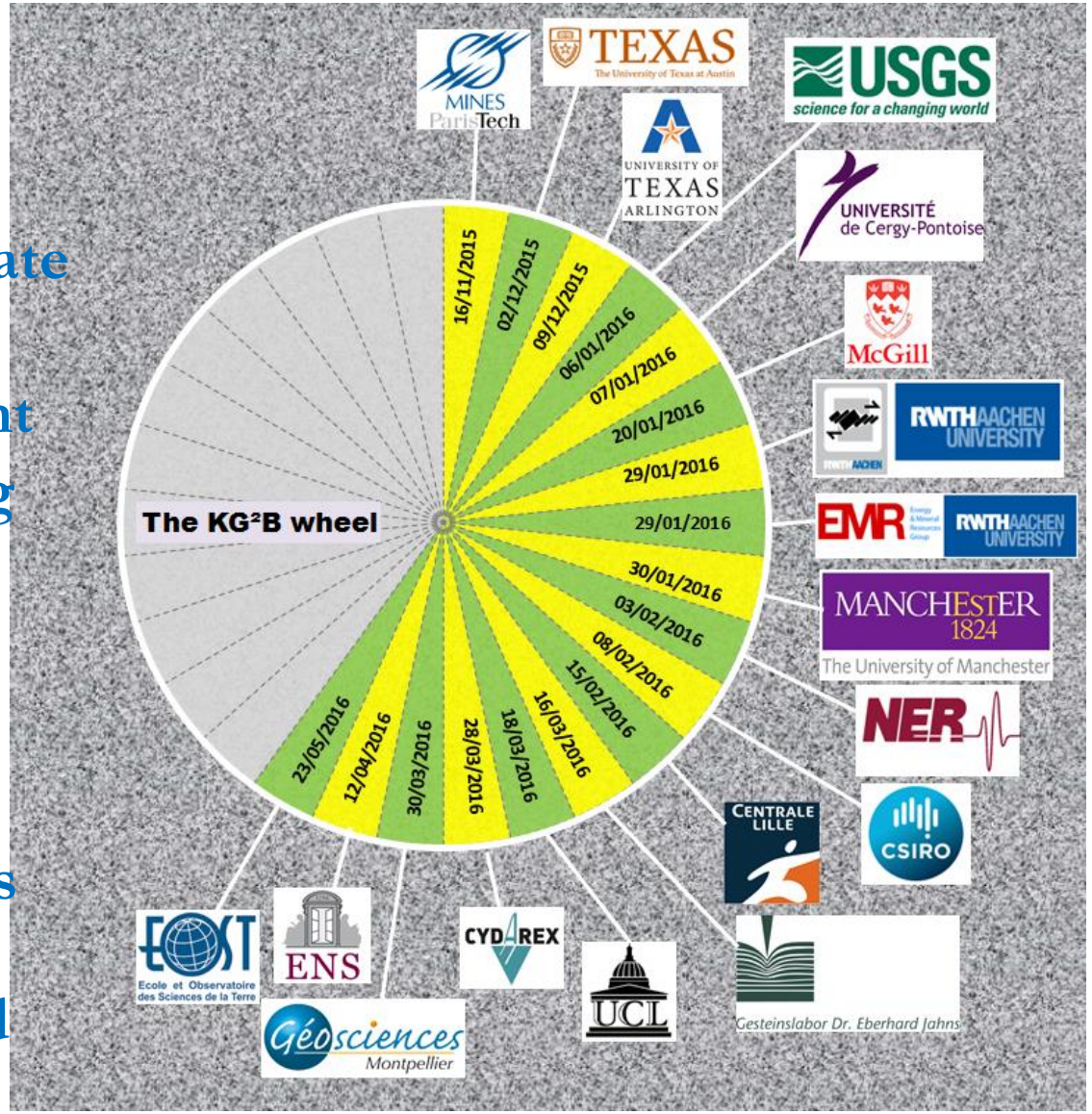

Porosity: 0.80±0.42% (N=31)
Permeability: 1.11±0.57 μD (N=35)

MICP

Porosity: 0.59%
Permeability: 1.08 μD

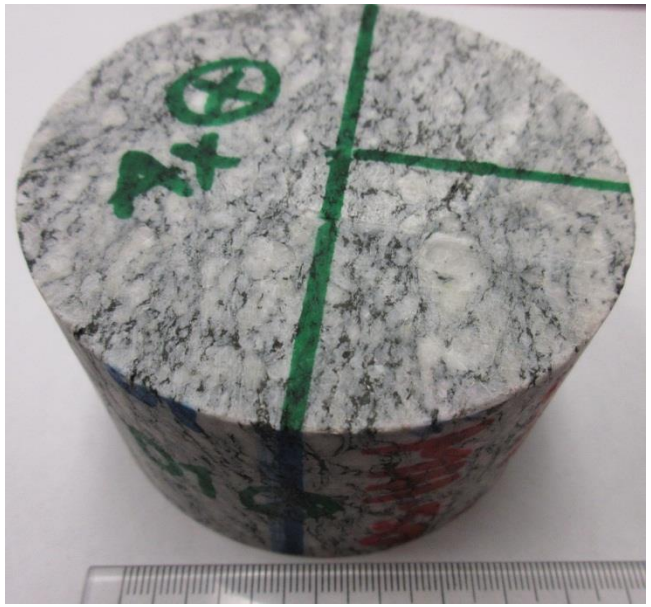

K for Grimsel Granodiorite Benchmark

David et al., GJI, 2018a, b

Multiple nm-μm Pore Systems

Shengli Oilfield, Sinopec

Liye#1

3782.63 m

GRI: #20 - #35 mesh

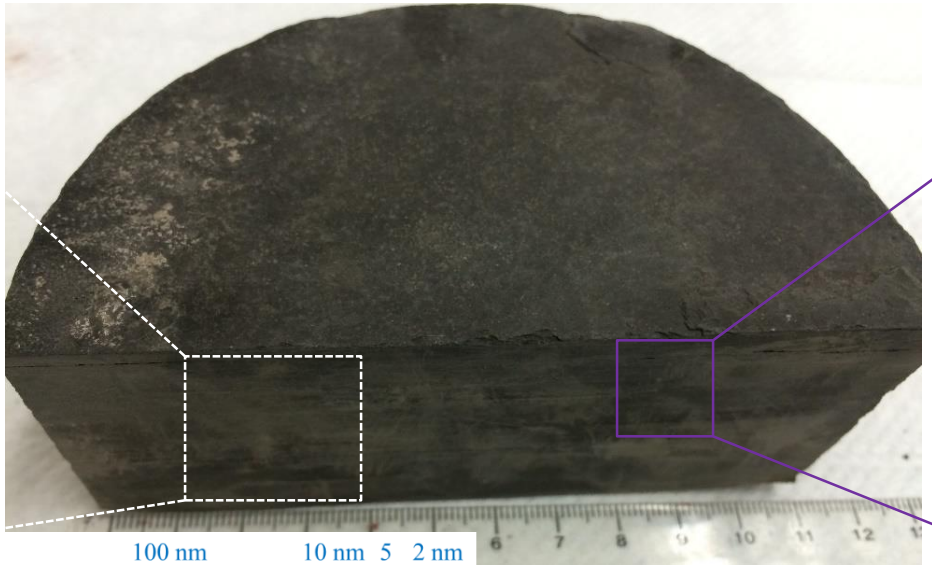

MICP: cube

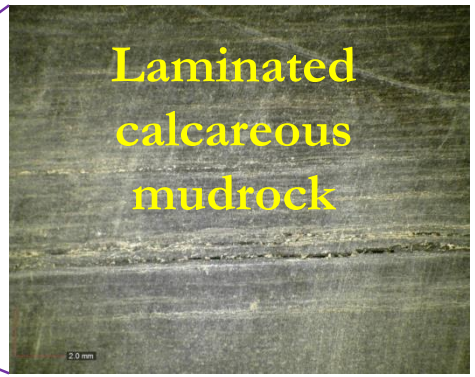

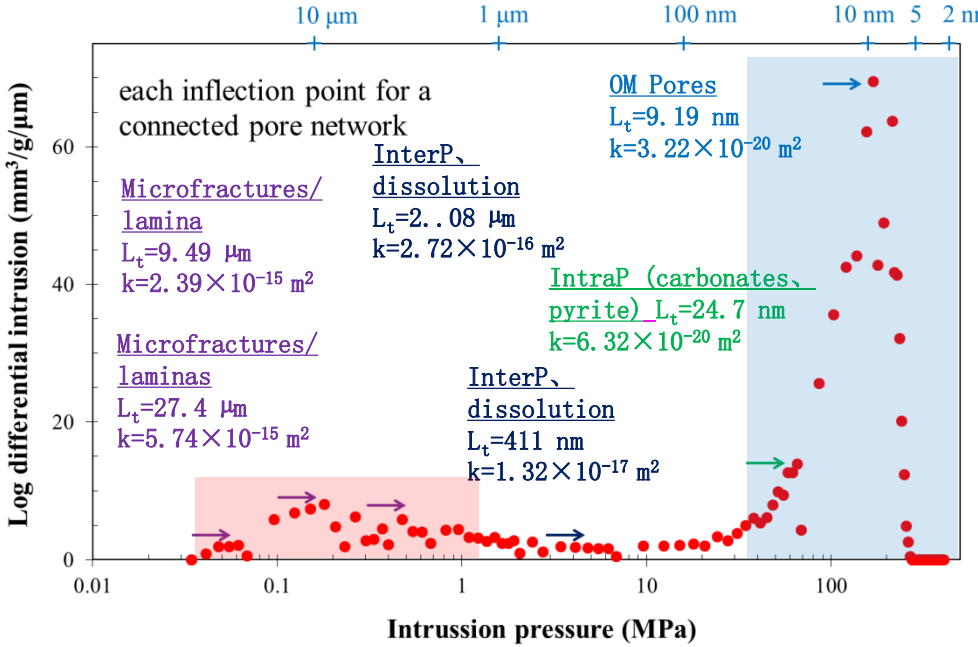

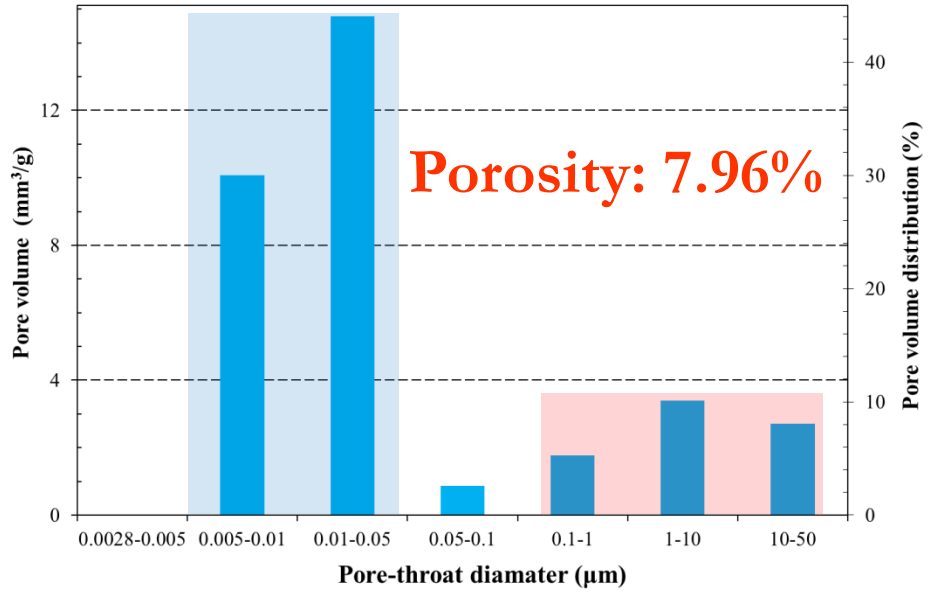

Hu et al., Petro. Explor. Develop., 2017

UNIVERSITY OF TEXAS ARLINGTON

Fracture Apertures: μm-CT vs. MICP

Shengli Oilfield

laminated

calcareous

mudrock

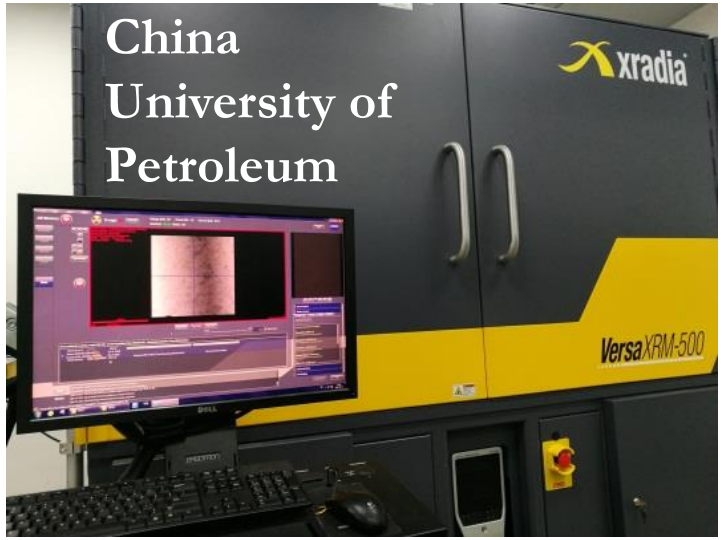

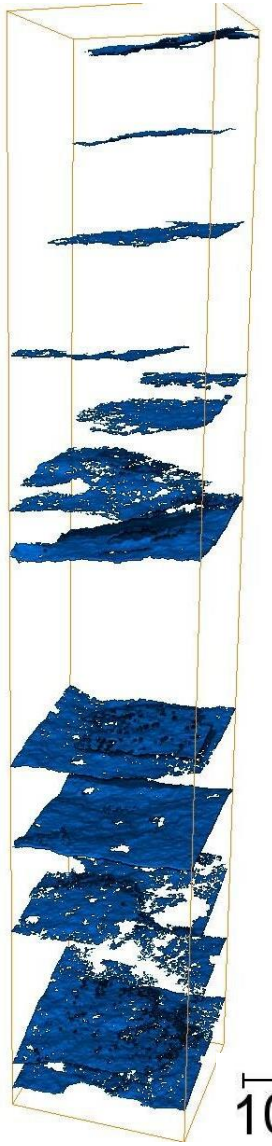

μm CT

16.18 μm 6.35 μm

MICP

0.71 - 27.4 μm

UNIVERSITY OF TEXAS ARLINGTON

Wood's Metal Intrusion, Imaging, and Mapping

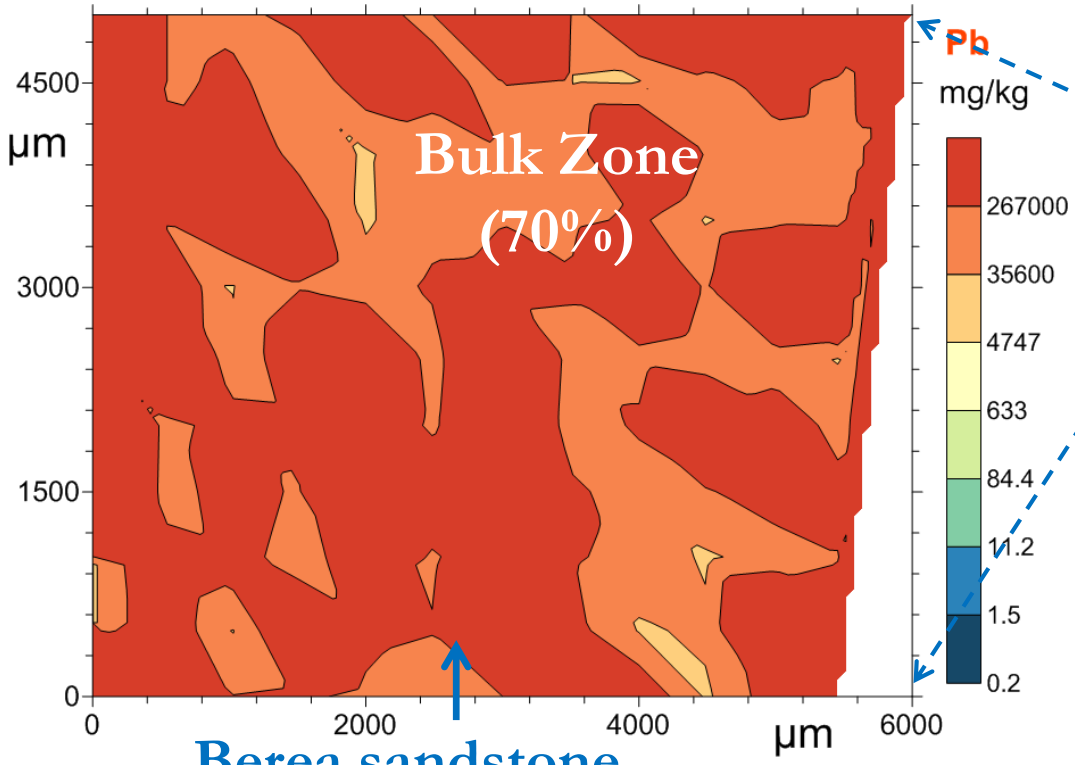

Berea sandstone

Median pore-throat size: 23.8 µm

Connectivity: good

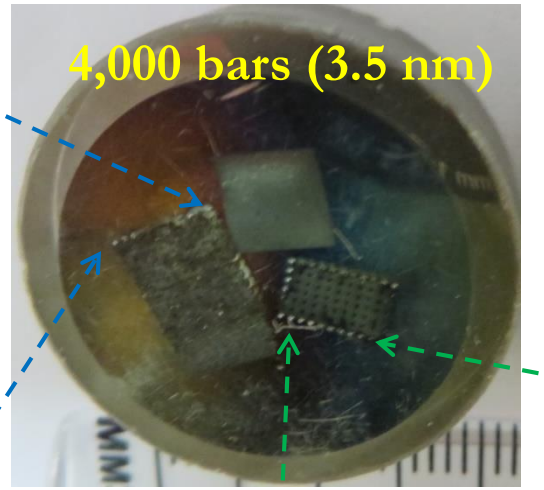

Leibniz Universität Hannover

Stefan Dultz

EMPA Materials Science & Technology

Josef Hoffmann

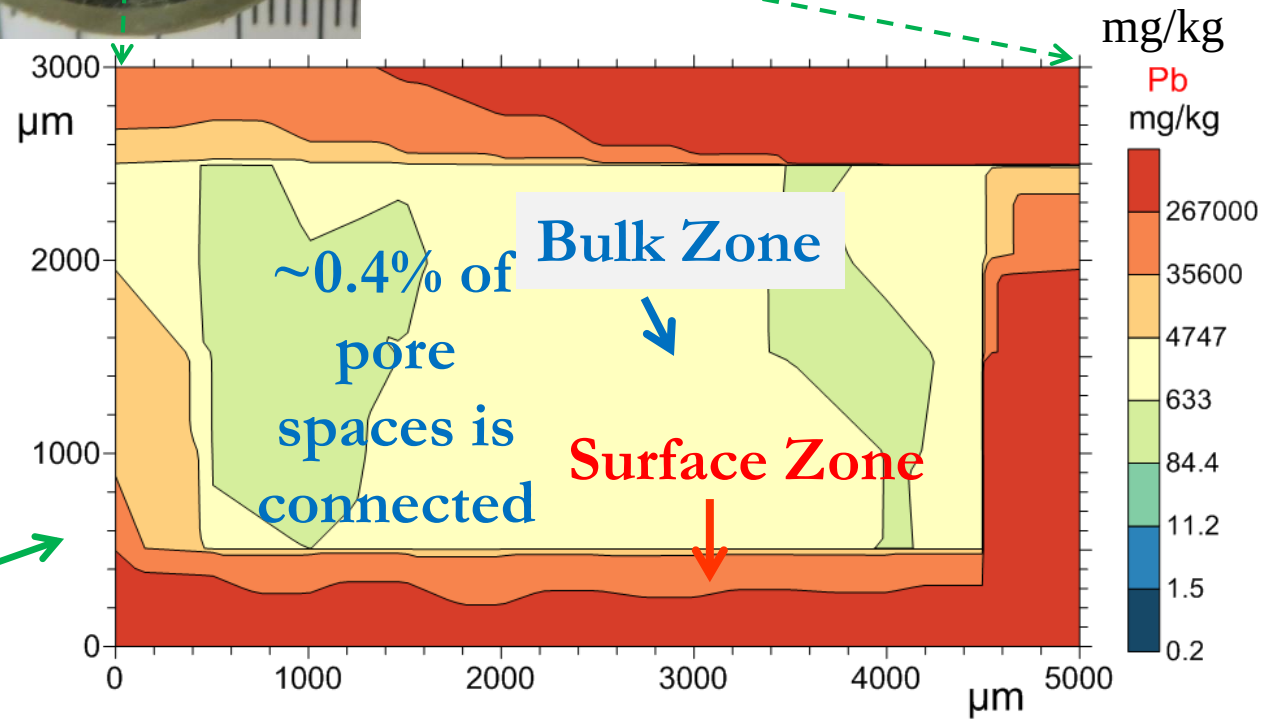

Barnett (Blakely #1 7136', limestone)

Median pore-throat size: 22.4 nm

Connectivity: poor

Wood's Metal Intrusion, Imaging, and Mapping

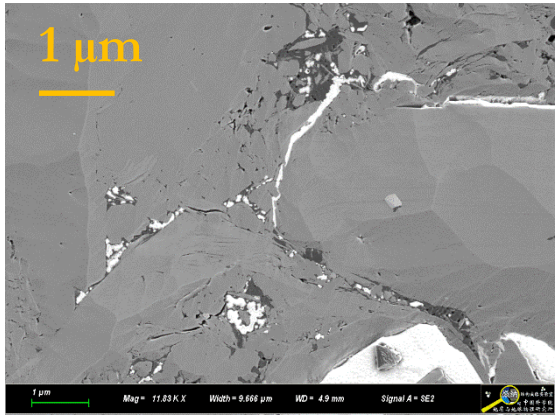

6,000 bars
(2.35 nm)

Barnett shale (Blakely #1 7,219') with cracks

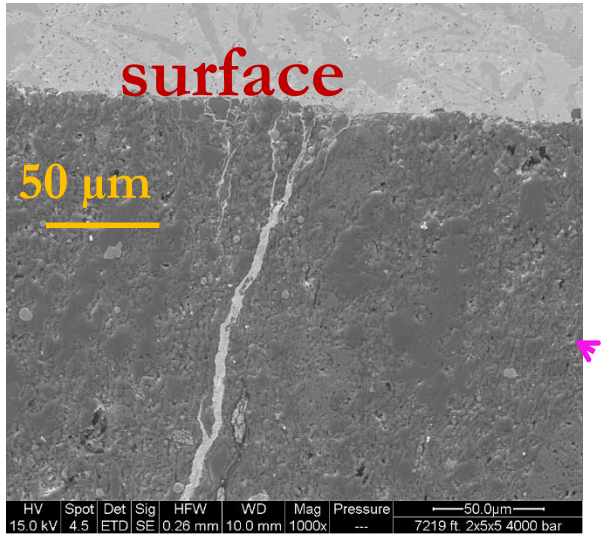

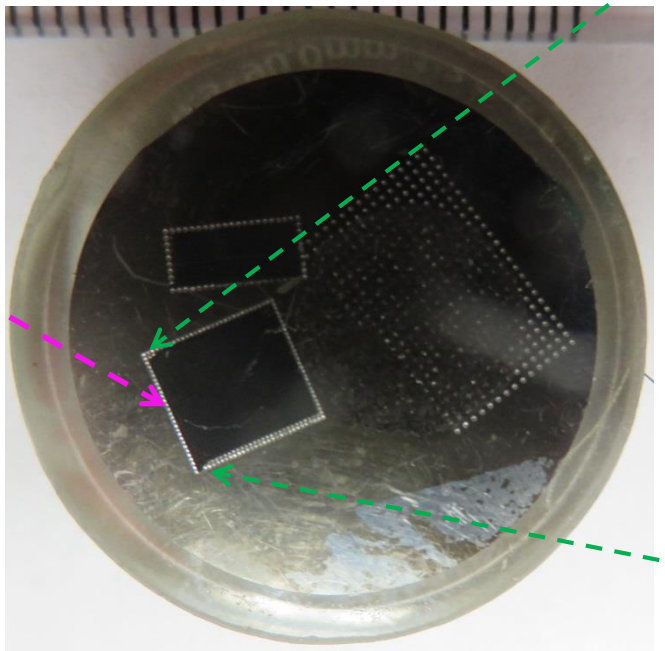

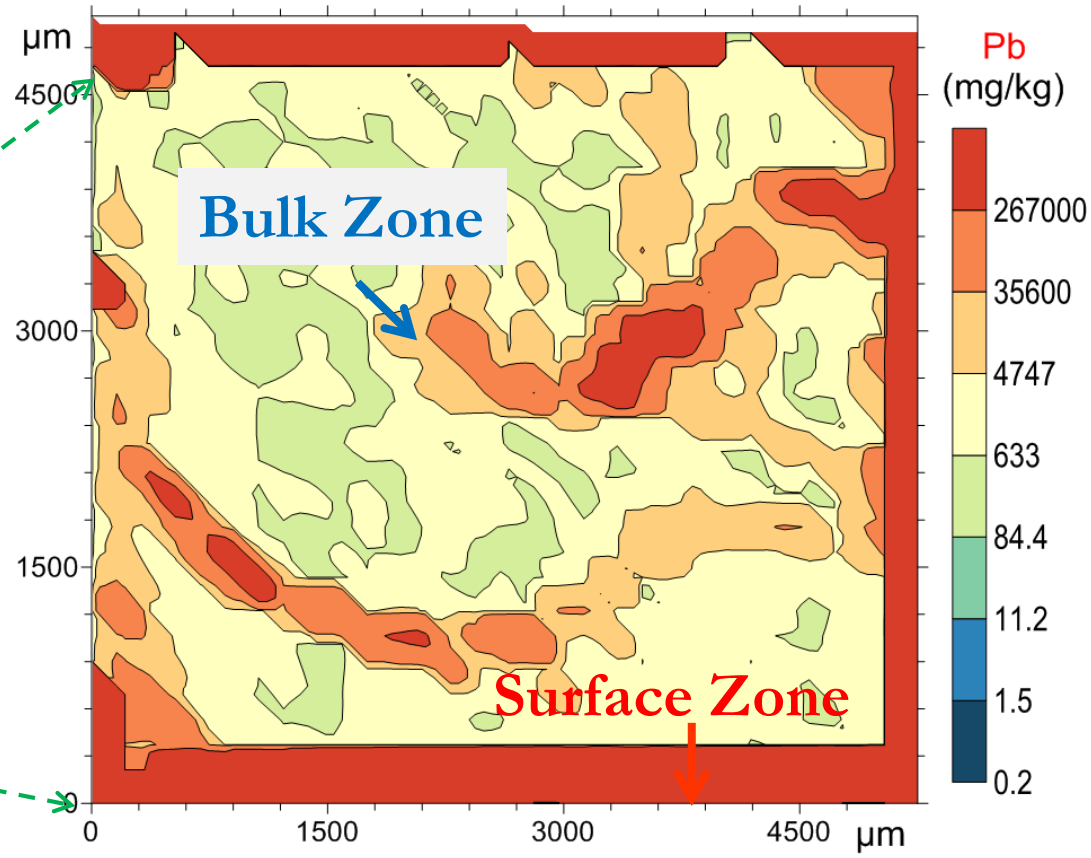

Hu et al., JCH, 2012; JGR, 2015

UNIVERSITY OF TEXAS ARLINGTON

Mixed Wettability and Associated Pore Structure

- Dalmatian wettability behavior
- Variable at um scale
- Complex interplay of wettability and pore size

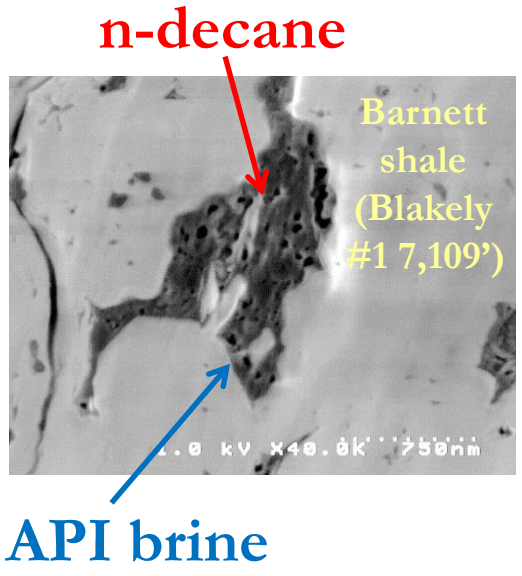

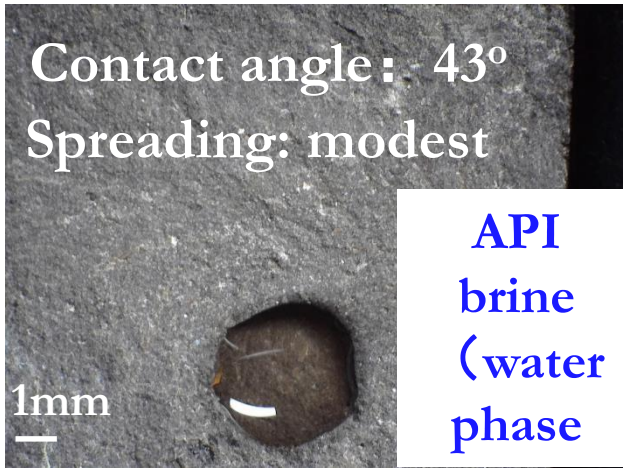

Fluid spreading behavior in a typical shale

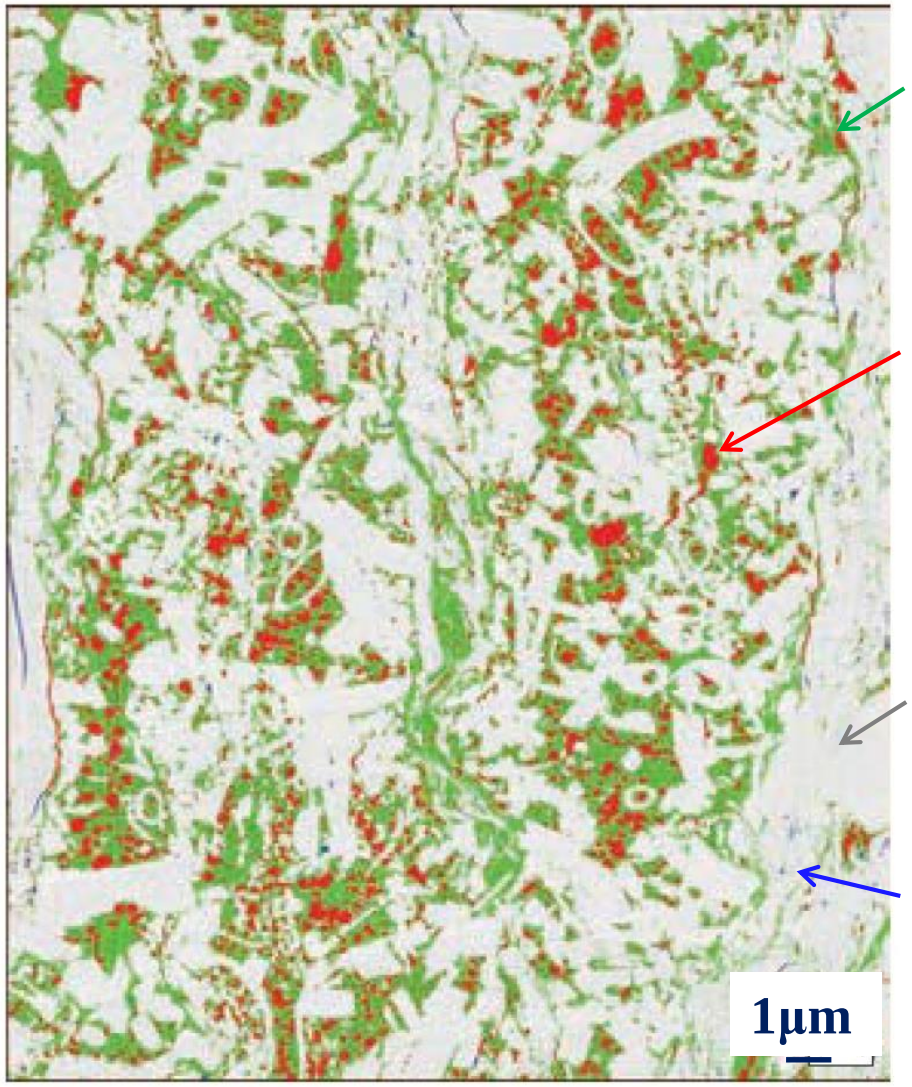

Wolfcamp: SEM (Wall et al., 2016)

UNIVERSITY OF TEXAS ARLINGTON

Wettability-based Fluids and Tracers

- API brine (8 wt% NaCl+2 wt% $CaCl_2$) [*water-wet*]
  - ✓ ReO_4^- (0.553 nm)
  - ✓ Anionic Sb-complex (0.89 nm)
  - ✓ Cationic Ru-complex (1.0 nm)
  - ✓ CdS nanoparticles (5–10 nm)

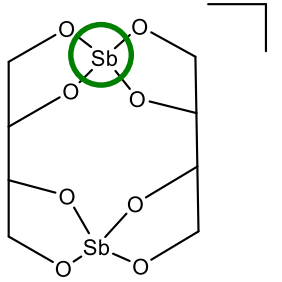

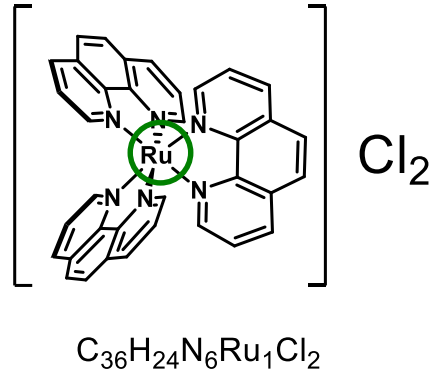

$C_{36}H_{24}N_6Ru_1Cl_2$

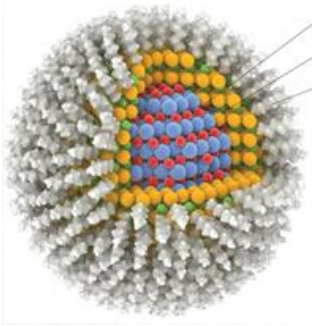

CdS (5–10 nm)

- n-decane: toluene [*oil-wet*]
  - ✓ Organic-I
  - ✓ Organic-Re
  - ✓ CeF_3 nanoparticles (10–12 nm)

0.23 nm

1.393 nm × 0.287 nm × 0.178 nm

$CH_3(CH_2)_8CH_2I$

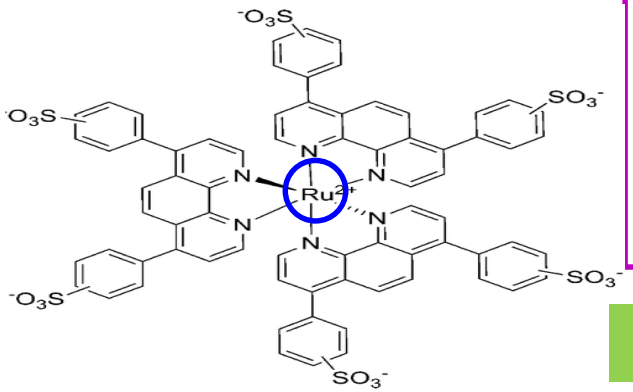

0.85 nm

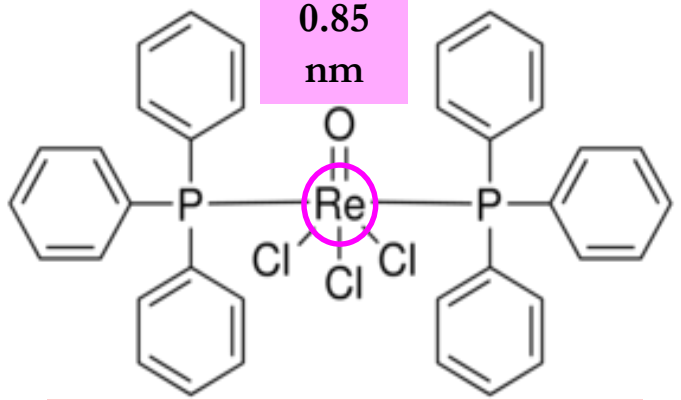

1.273 nm × 0.919 nm × 0.785 nm

- Tetrahydrofuran–zewittering
  - ✓ Ru-complex (2.42 nm)

Hu et al., J. Nano. Nanotech., 2017

UNIVERSITY OF TEXAS ARLING

Different Tracer Tests for Process-Level Understanding

Imbibition

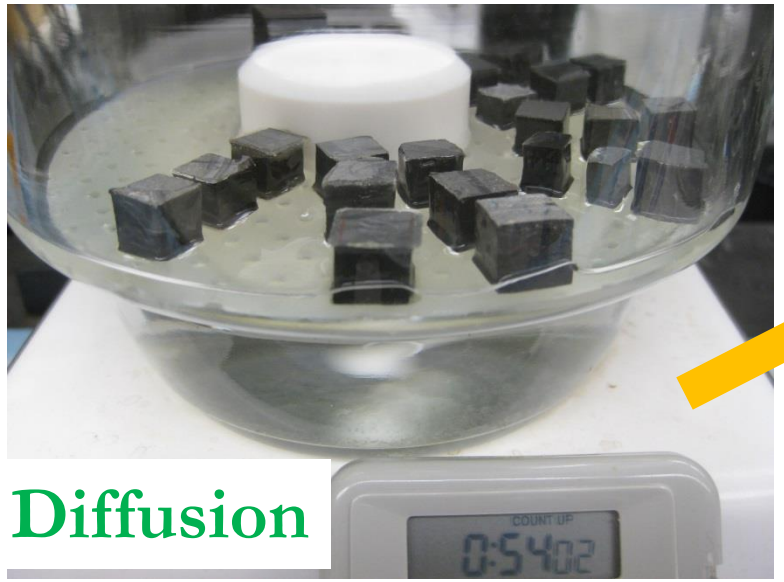

Diffusion

Laser Ablation-Inductively Coupled Plasma-Mass Spectrometry（LA-ICP-MS）

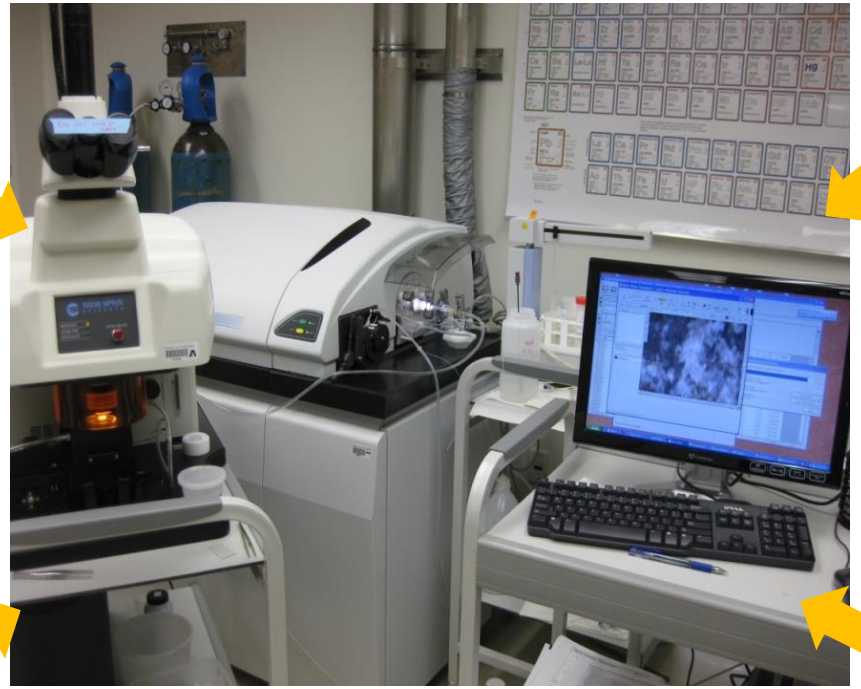

Hu et al, Vadose Zone J., 2002

Vacuum saturation

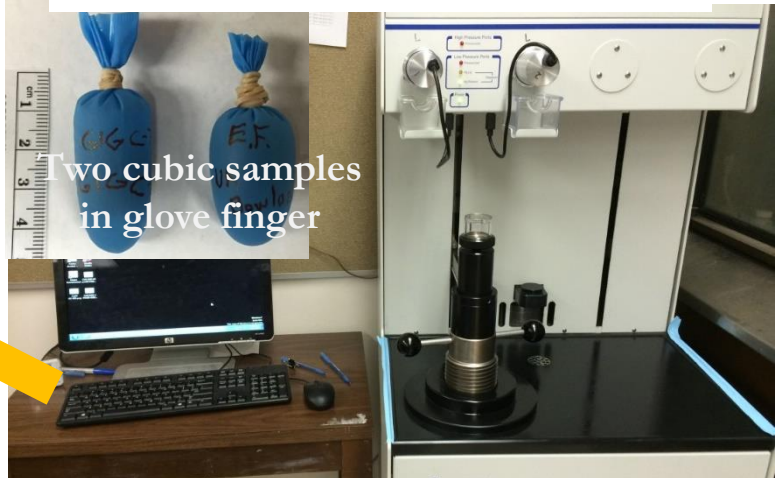

High-pressure impregnation

UNIVERSITY OF TEXAS ARLINGTON

Laser Ablation-ICP-MS Tracer Mapping

10 mm-sided cube

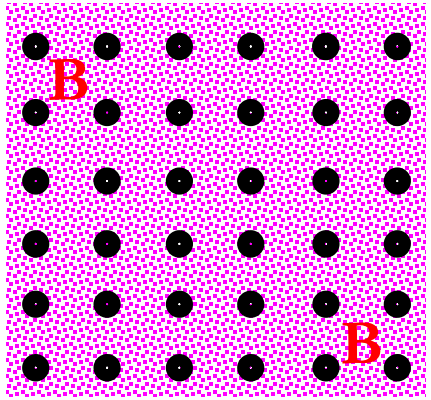

Bottom (tracer-contacted) face conc. check

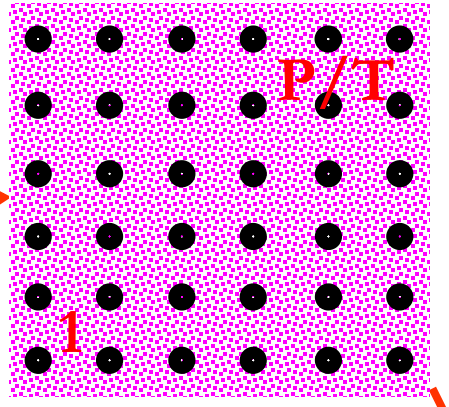

Conc. check of top face (either Parallel or Transverse to lamination)

3D mapping

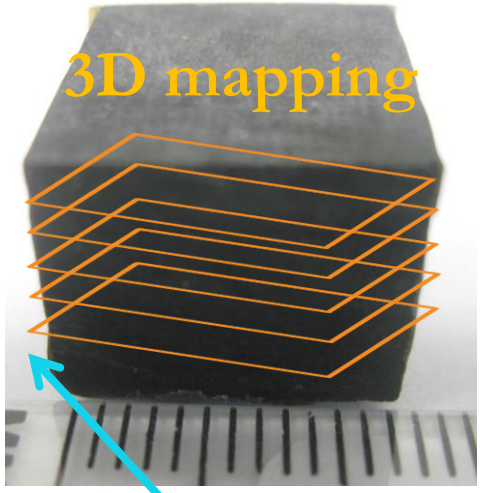

Hu et al., JGR, 2015

Cut the sample dry to expose the interior face

Interior face(2D mapping)

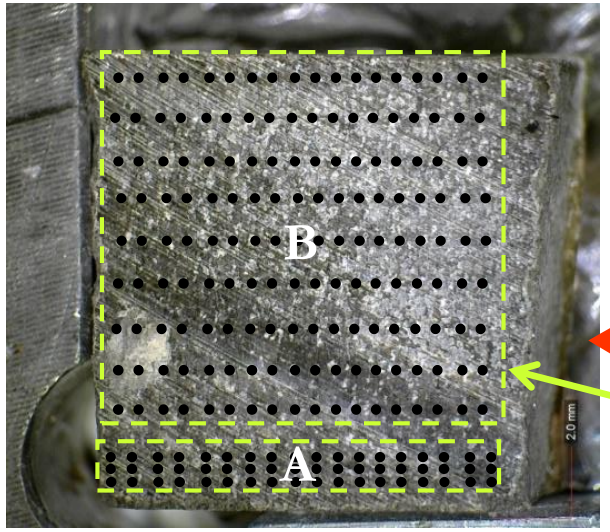

Remove epoxy on the wall to map side face

Tracer mapping grids

UNIVERSITY OF TEXAS ARLINGTON

Non-wetting Fluid：Effective Porosity Effect

Re background: 1.29±1.24 mg/kg

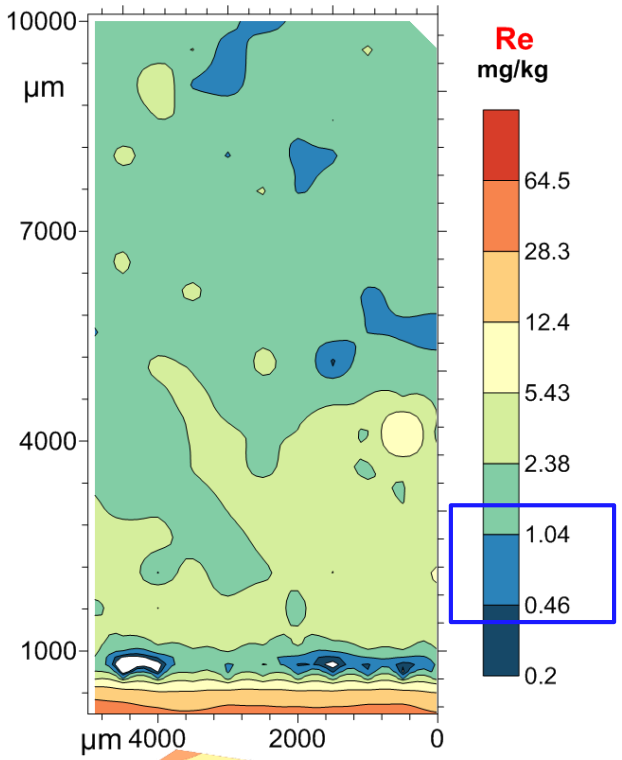

Cs background: 8.85±4.20 mg/kg

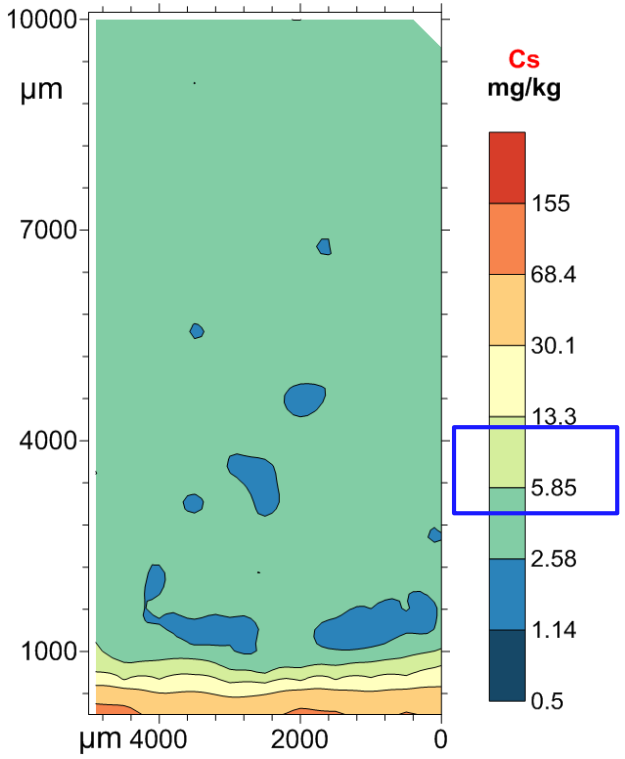

Ce background: 51.0±33.6 mg/kg

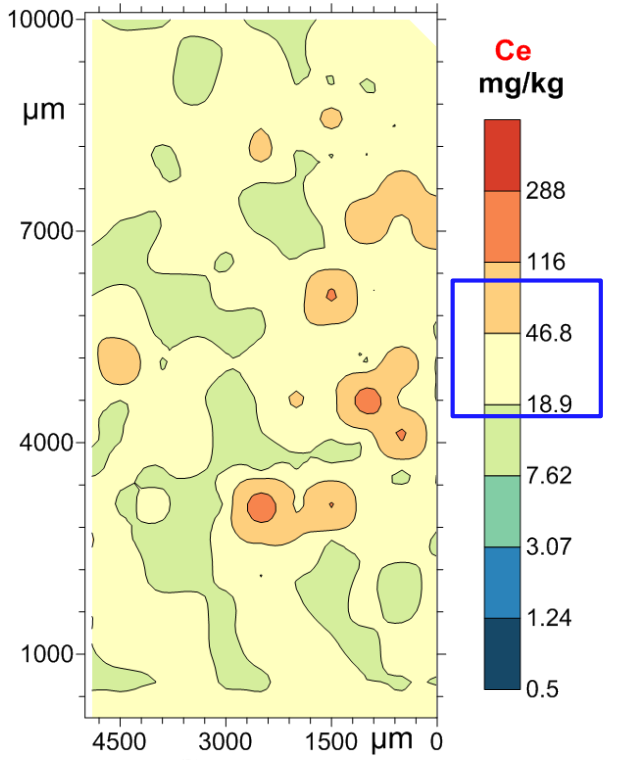

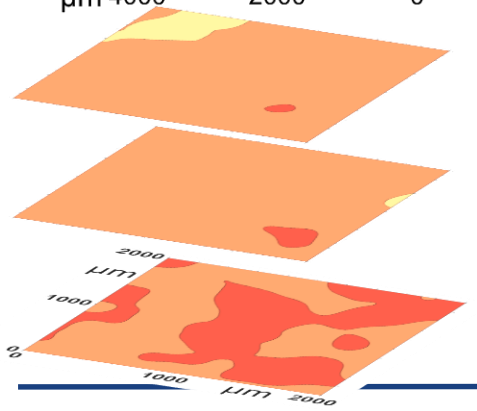

5–71 μm

1–5 μm

0–1 μm

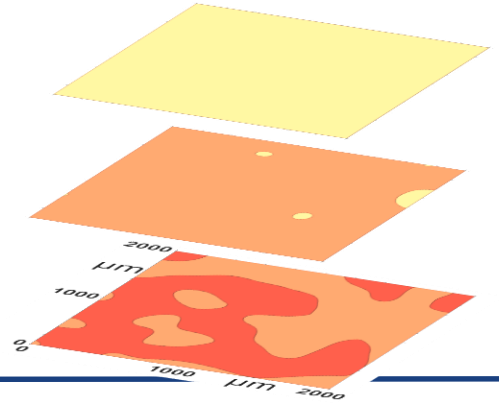

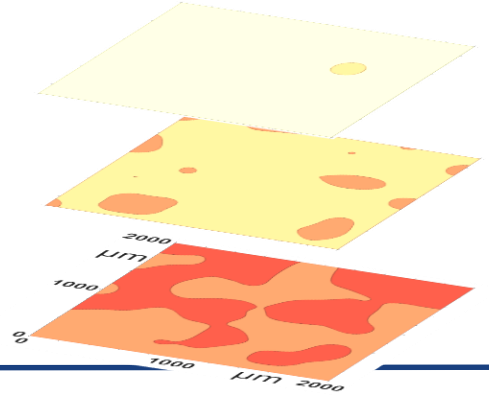

Barnett 7109’
Brine
Imbibition
94 hrs

Wetting Fluid：Molecular Size Effect

Eagle Ford shale

n-decane

Vac sat + High-pressure intrusion

$CH_3(CH_2)_8CH_2I$

0.23 nm

1.393 nm × 0.287 nm × 0.178 nm

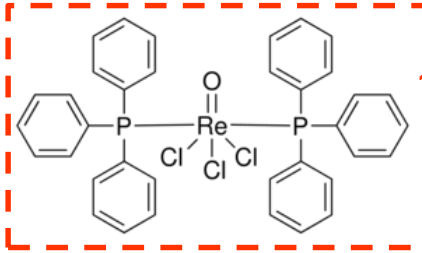

1.273 nm × 0.919 nm × 0.785 nm

0.85 nm

I bkgd: 2.54±2.67 mg/Kg

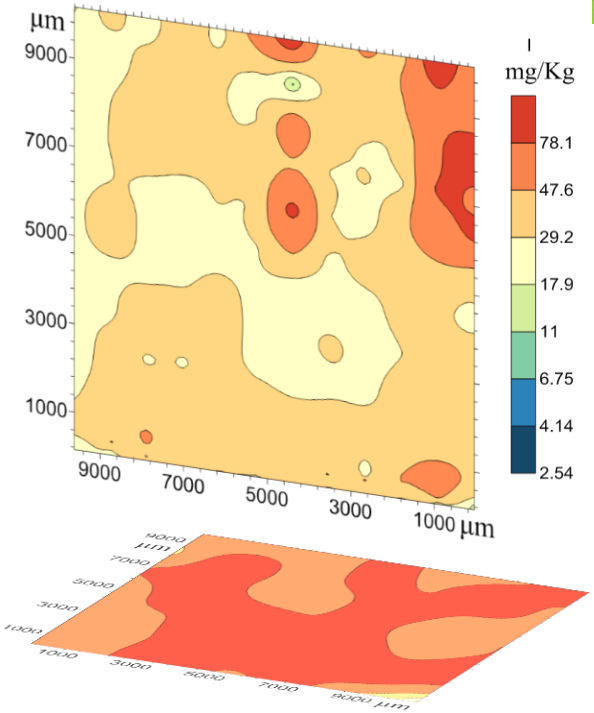

Oil-wet pores： 2.8-20nm pore throat dia.

H_2O: 0.32 nm

CH_4: 0.38 nm

Aromatics: 1-3 nm

Asphaltene: 5-10 nm

(Nelson, 2009)

Re bkgd：1.55±1.46 mg/Kg

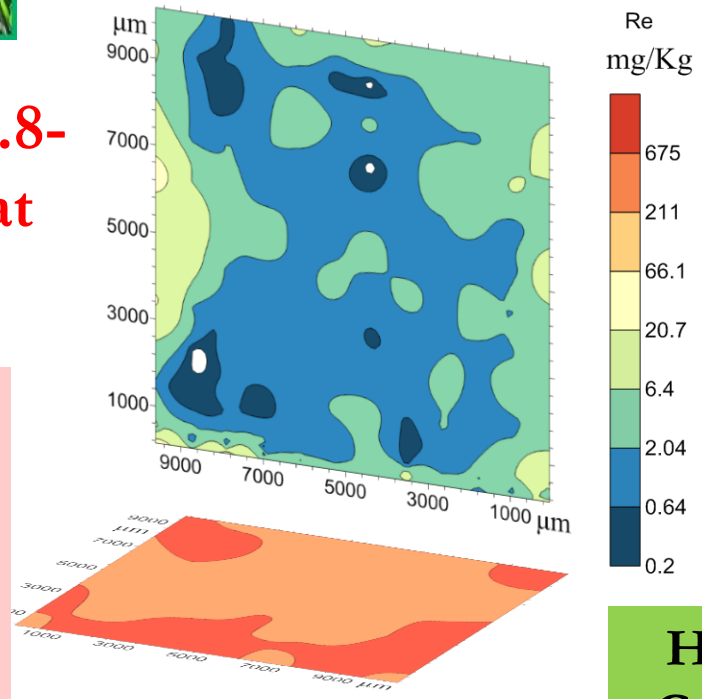

Hu et al., Geofluids, 2018

UNIVERSITY OF TEXAS ARLINGTON

Small Angle Neutron Scattering (SANS)

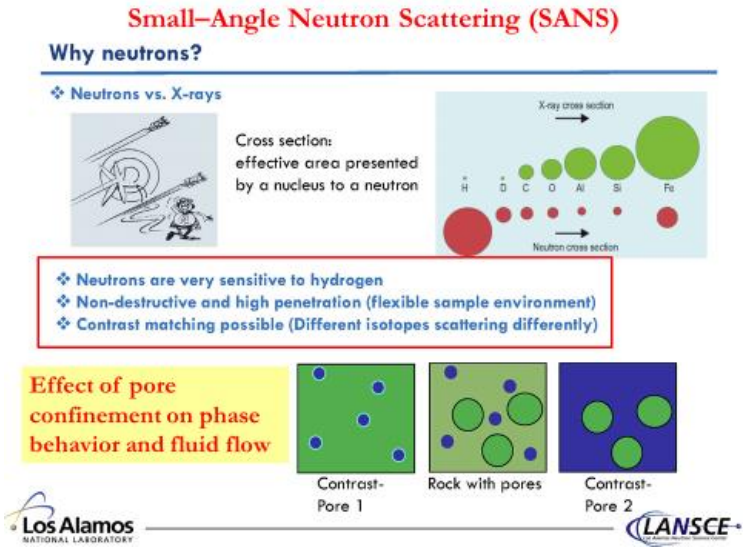

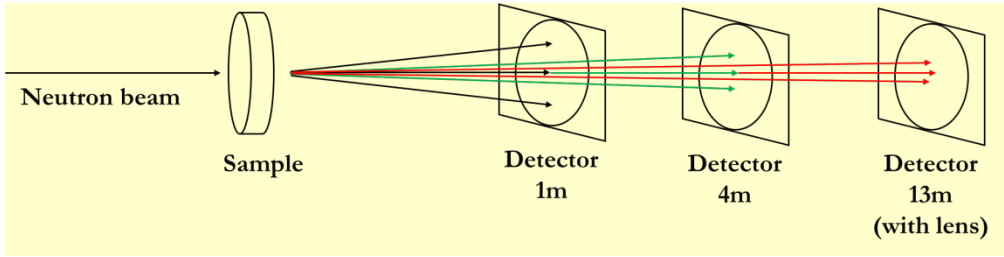

- Detect both connected and closed pores
- Obtain full-scale nm-μm pore diameters
- Quantify hydrophilic vs. hydrophobic pore space
- Investigate reservoir P-T condition

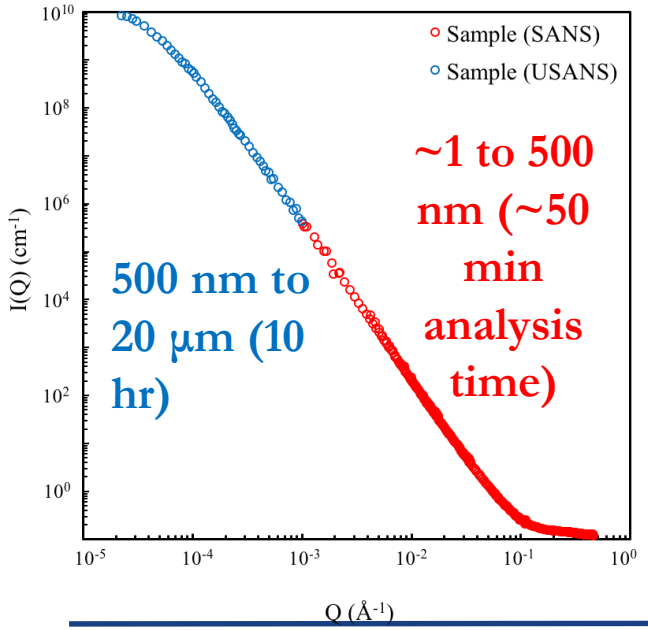

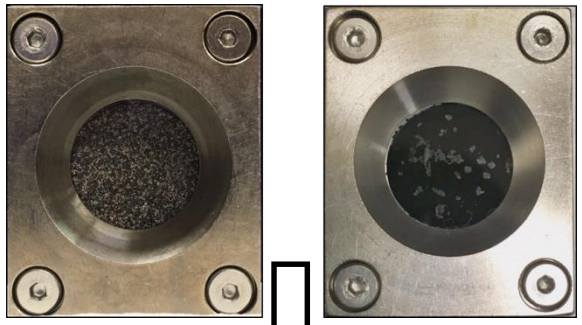

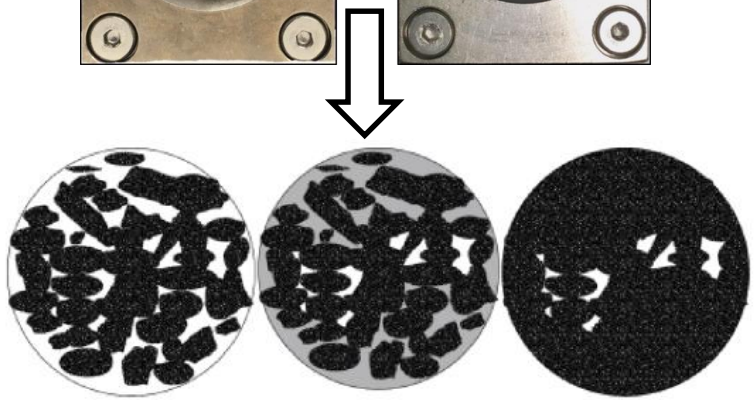

d–H_2O
d–decane
d–THF

Yang et al., 2017; Sun et al., 2017; Zhao et al, SR, 2017; Zhang et al., 2019

UNIVERSITY OF TEXAS ARLINGTON

(U)SANS: Fluid-Wettable Pore Space

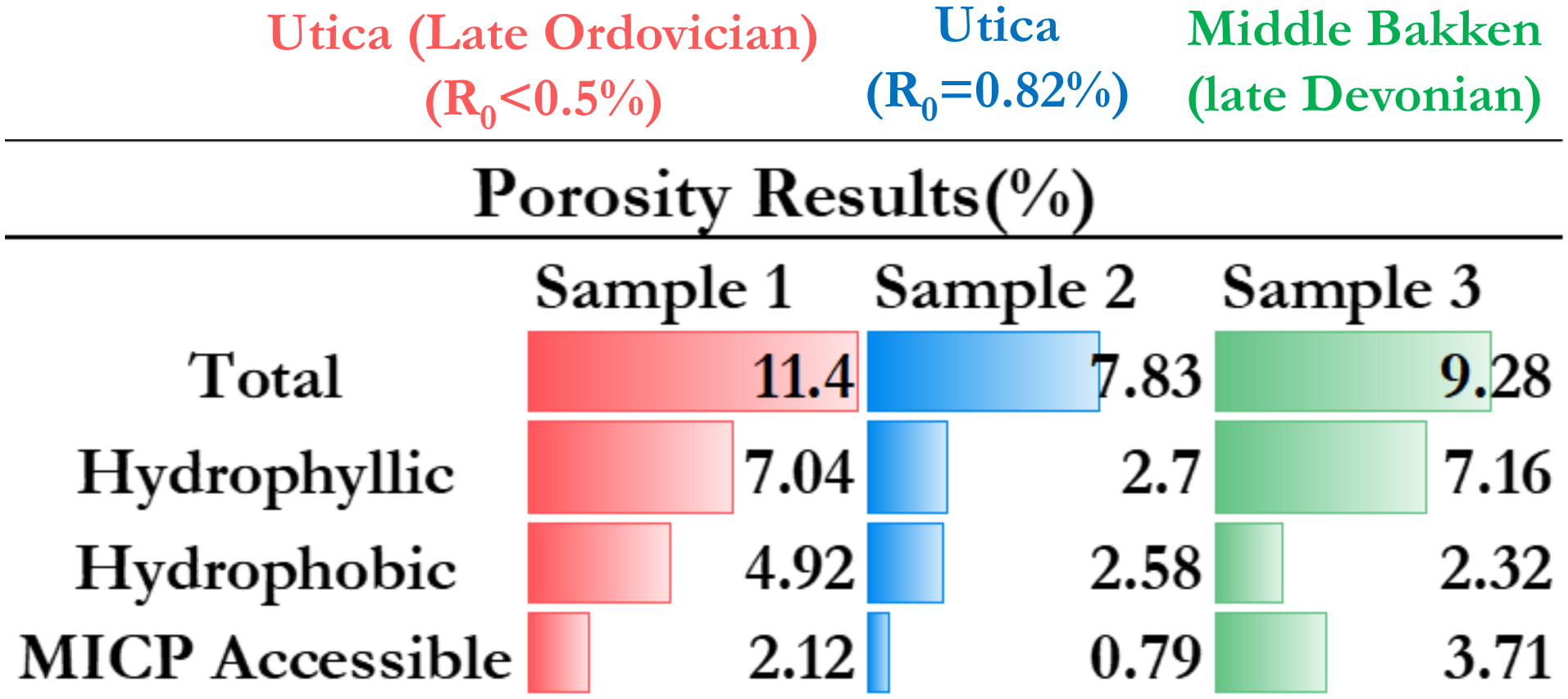

Zhang et al., 2019 (under prep.)

	Formation	TOC	MICP (1cm cube)	(U)SANS (grains: 177-500 µm)	MICP (grains: 177-500 µm)	
				(1.1 nm – 20 µm)	(3.4nm - 50 µm)	(3.4 nm - 10 um)
Upper Bakken						
Sample #4	Bakken	13.7wt.%	2.29%	11.69%	13.20%	11.10%

UNIVERSITY OF TEXAS ARLINGTON

Production Decline in Log-Log Space

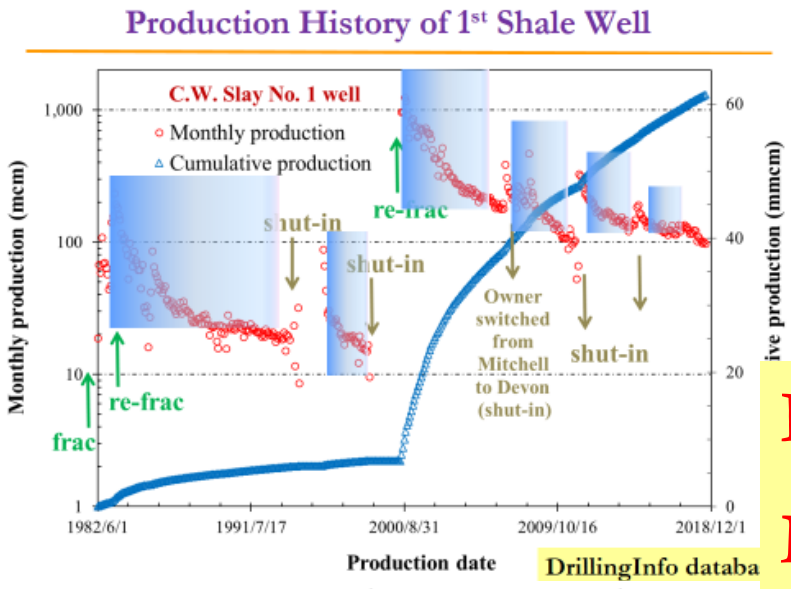

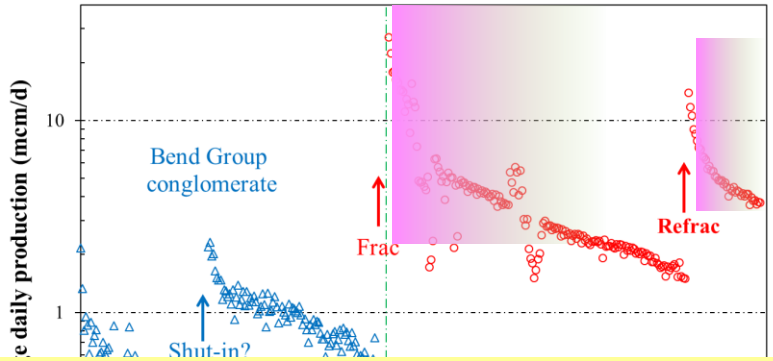

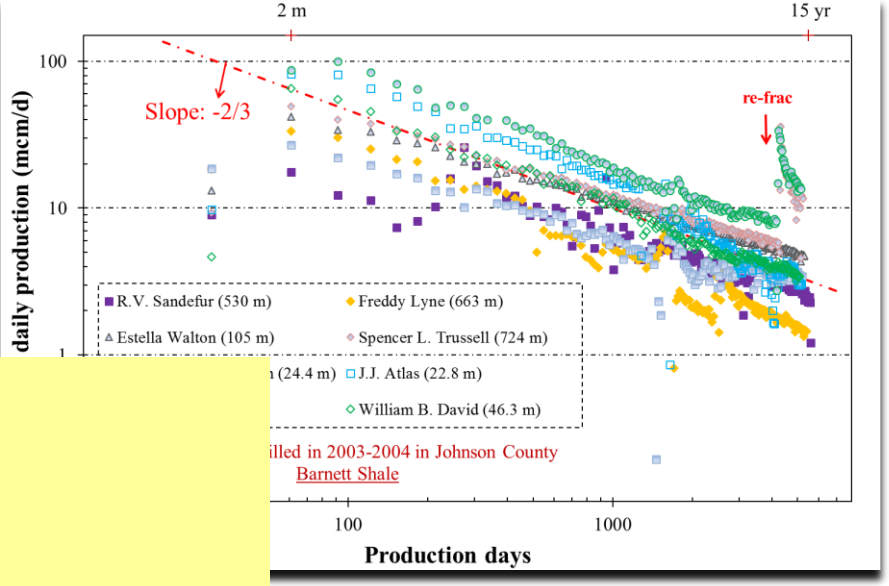

Fractures： -1

Matrix： -1/2 or -1/4

Fracture-Matrix interaction： -2/3

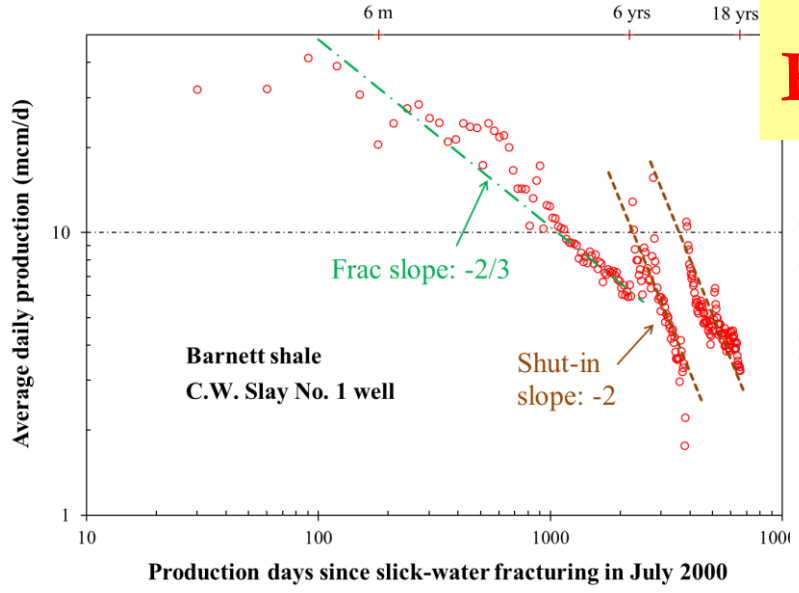

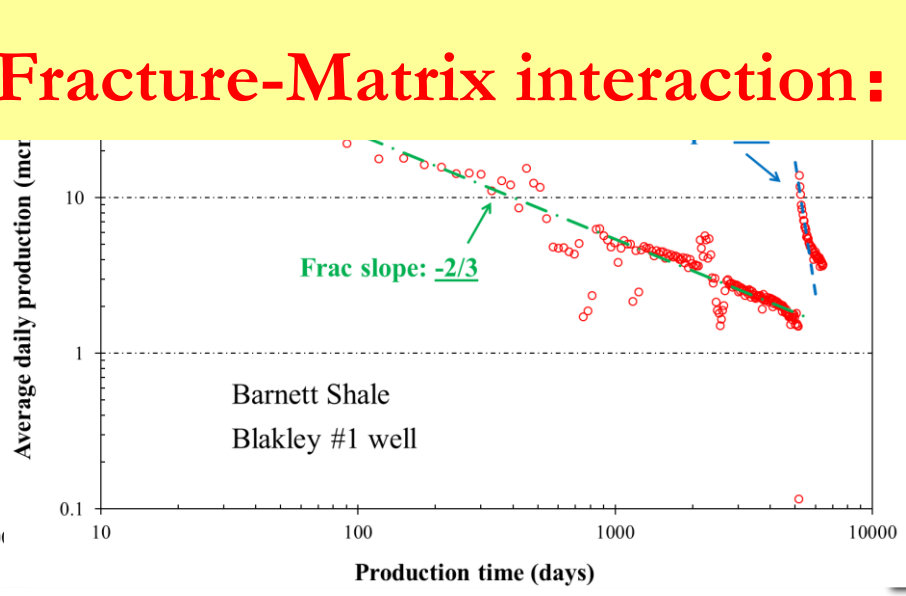

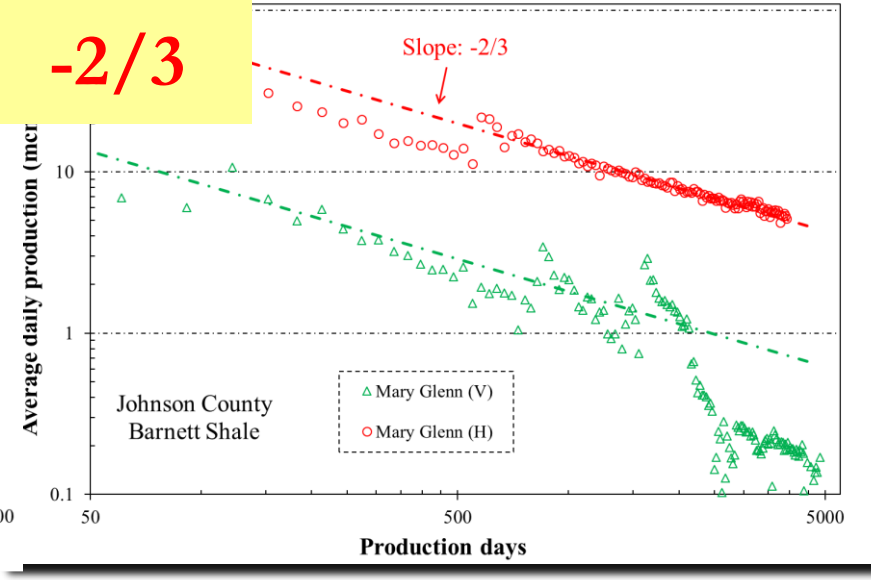

UNIVERSITY OF TEXAS ARLINGTON

Summary and Application

- Dual connectivity at ~500 μm from sample edge (rapid initial decline & low recovery; completions for complex fracture network; refrac; shut-in)
- Mixed wettability at μm scale; oil than water (modification for enhanced recovery)
- Dual flow paths in 3-D space: >10-50 nm hydrophilic pore network at slow rate; ~5 nm hydrophobic pore network with rapid rate but size exclusion (production of small-sized hydrocarbons)